INFORMATION TO USERS

This material was produced from a microfilm copy of the original document. While the most advanced technological means to photograph and reproduce this document have been used, the quality is heavily dependent upon the quality of the original submitted.

The following explanation of techniques is provided to help you understand markings or patterns which may appear on this reproduction.

1. The sign or "target" for pages apparently lacking from the document photographed is "Missing Page(s)". If it was possible to obtain the missing page(s) or section, they are spliced into the film along with adjacent pages. This may have necessitated cutting thru an image and duplicating adjacent pages to insure you complete continuity.

2. When an image on the film is obliterated with a large round black mark, it is an indication that the photographer suspected that the copy may have moved during exposure and thus cause a blurred image. You will find a good image of the page in the adjacent frame.

3. When a map, drawing or chart, etc., was part of the material being photographed the photographer followed a definite method in "sectioning" the material. It is customary to begin photoing at the upper left hand corner of a large sheet and to continue photoing from left to right in equal sections with a small overlap. If necessary, sectioning is continued again — beginning below the first row and continuing on until complete.

4. The majority of users indicate that the textual content is of greatest value, however, a somewhat higher quality reproduction could be made from "photographs" if essential to the understanding of the dissertation. Silver prints of "photographs" may be ordered at additional charge by writing the Order Department, giving the catalog number, title, author and specific pages you wish reproduced.

5. PLEASE NOTE: Some pages may have indistinct print. Filmed as received.

Xerox University Microfilms

300 North Zeeb Road
Ann Arbor, Michigan 48106

74-4000

BROCK, Fred Vincent, 1932-
EXPERIMENTAL ANALYSIS OF PROPELLER ANEMOMETER
DYNAMIC PERFORMANCE.

The University of Oklahoma, Ph.D., 1973
Physics, meteorology

University Microfilms, A XEROX Company, Ann Arbor, Michigan

THIS DISSERTATION HAS BEEN MICROFILMED EXACTLY AS RECEIVED.

THE UNIVERSITY OF OKLAHOMA

GRADUATE COLLEGE

EXPERIMENTAL ANALYSIS OF PROPELLER ANEMOMETER DYNAMIC PERFORMANCE

A DISSERTATION

SUBMITTED TO THE GRADUATE FACULTY

in partial fulfillment of the requirements for the

degree of

DOCTOR OF PHILOSOPHY

BY

FRED VINCENT BROCK

Norman, Oklahoma

1973

EXPERIMENTAL ANALYSIS OF PROPELLER ANEMOMETER
DYNAMIC PERFORMANCE

APPROVED BY

Claude E. Archer

Ralph Smith

Amos Edel

Edward F. Blick

DISSERTATION COMMITTEE

1. Introduction

The dynamic performance of cup and propeller anemometers has been extensively studied and reported in the literature. They are commonly used for the measurement of small scale atmospheric motions because they are relatively inexpensive, reliable, and easy to use. However the dynamic performance of mechanical anemometers is often marginal for such applications so the data must be corrected for the sensor response characteristics. Since these corrections can be quite large it is necessary to have a good differential equation model for the anemometer dynamic performance.

A linear model is frequently used as a first approximation to anemometer dynamic performance but dynamic nonlinearity has often been observed, most noticeably in overrun or overestimation of the mean in turbulent flow. It is assumed in this study that propeller anemometers are linear in the static sense above the threshold region. This means that in steady flow, well above the propeller starting speed, and with proper calibration applied, the anemometer output is equal to the input.

Izumi and Barad (1970) made a comparison study of a cup anemometer, a sonic anemometer and a hot-wire anemometer. Each was calibrated in a wind tunnel and then mounted on a tower at 5.66 m. Average values were calculated over 15 minute intervals when the wind direction was in a quadrant to minimize tower interference. They did not report wind spectra or even the variance but only mean values. They found the cup anemometer consistently overestimated the wind speed compared to the sonic or hot-wire anemometers by 8-12% with only slight variation by stability class. This is a little surprising since one would expect the overestimation of the mean to be a function of the average wind speed and of the spectrum. At times the overestimation of the mean should be nearly zero. The speed range of their observations was from 2 to 9 m sec^{-1}.

Hyson (1972) observed overestimation of the mean in field comparison of cup and hot-wire anemometers. He found that in neutral conditions at a height of 1.5 m, the overrun percentage was 16.7 $(\sigma_V/V - 0.12)$ for $\sigma_V/V \geq 0.12$. He observed overrun up to 3% and found the overrun percentage decreased with height. In one case it decreased from about 1% at 1 m to 0.5% at 4 m to 0.2% at 8 m. This is to be expected since the average wind speed increased rapidly with height in the first few meters.

Many investigators, e.g., Hyson (1972), Kondo, Naito and Fujinawa (1971) and Acheson (1970) attempted to determine nonlinear anemometer response models from step function wind tunnel tests. In these tests the tunnel speed is held constant and the anemometer is released from a braked (usually stopped) or overspeed condition. The response shows a noticeable deviation from the simple linear step function response which has the form $B + (A - B)e^{-t/\tau}$ where the initial and final anemometer speeds are A and B, respectively. This deviation may be partially obscured by experimental problems with anemometer release and by noise. But even without these problems, it is difficult to fit a model involving terms in V^2 and VV_i, where V and V_i are the anemometer and tunnel speed, respectively, when the tunnel speed is constant. Evidently a fluctuating wind speed is required to produce more noticeable nonlinear response. An analysis based on relatively small deviations from linear response produced in a wind tunnel does not find ready acceptance since it is easy to dismiss the results as biased by experimental error or as being not representative of atmospheric conditions.

Commenting on the results of models derived from analysis of constant tunnel flow data, Acheson (1970) concludes: "However, differences still remain to which the only obvious resolution lies in performing the measurements necessary to determine which differential equation best approximates the sensor at hand."

It is difficult to run a test in the atmosphere that will provide data for critical analysis of nonlinear models. The anemometers to be compared do not "see" the same input and can be compared only statistically. As shown by previously quoted results, it is possible to detect overestimation of the mean in the atmosphere but that is insufficient for model fitting. Spectrum analysis is also insufficient due to the failure of the superposition principle for nonlinear models. Another difficulty is the normal lack of stationarity in the atmosphere.

These problems were bypassed by the use of a wind tunnel at the National Center for Atmospheric Research which could generate variable, controlled tunnel speeds in the appropriate amplitude/frequency range to excite nonlinear response characteristics of a propeller anemometer. An experiment, described below, was designed for this wind tunnel to generate data which could be used for objective analysis of various nonlinear anemometer performance models.

2. Mathematical Models

The linear model often used to describe the dynamic performance of cup and propeller anemometers, for example (MacCready, 1970) is

$$\tau \frac{dV}{dt} = V_i - V \tag{1}$$

where
τ = time constant
V = output wind speed
V_i = input wind speed
t = time.

Schubaer and Adams (1954) found in wind tunnel tests that the time constant τ is an inverse function of wind speed,

$$\tau = \lambda V_i^{-1} \tag{2}$$

where the new constant λ is called a distance constant. If (2) were substituted into (1), the result would be a non-linear model. To preserve linearity with all the attendant advantages, the average wind speed is used so $\tau = \lambda \overline{V}_i^{-1}$. This is a reasonable assumption when the turbulent fluctuations in the wind speed are small compared to the mean. In any event, it provides a very convenient linear reference model.

One nonlinear model, as mentioned above, results from substituting (2) into (1) which yields,

$$\lambda \frac{dV}{dt} = V_i(V_i - V). \tag{3}$$

This model was studied by Acheson (1970) who also suggested

$$\lambda \frac{dV}{dt} = V_i^{\,2} - V^2. \tag{4}$$

Ramachandran (1969) proposed

$$\lambda \frac{dV}{dt} = a_0 + a_1 V + a_2 V V_i + a_3 V_i^{\,2} \tag{5}$$

where a_0 is a coefficient related to friction. For immediate purposes, the friction term will be ignored which is reasonable when the wind speed is well above the anemometer threshold. Even ignoring a_0, (5) does not satisfy the requirement for static linearity which requires that $dV/dt = 0$ when $V = V_i$. In (5) when $dV/dt = 0$ the right side

$$a_1 V + a_2 V V_i + a_3 V_i^{\,2} = 0$$

leads to

$$V = - a_3 V_i^{\,2}(a_1 + a_2 V_i)^{-1}.$$

Ramachandran observed that some of the discrepancies in his results could be explained by letting the coefficient a_1 be a function of V. After redefining a_1,

$$\lambda \frac{dV}{dt} = a_1 V^2 + a_2 V V_i + a_3 V_i^{\,2} \tag{6}$$

satisfies the static linearity requirement of $a_1 + a_2 + a_3 = 0$.

The model proposed by Kondo, Naito, and Fujinawa (1971) is

$$\lambda \frac{dV}{dt} = V_i(V_i - (1 + \gamma)V) + \gamma V^2 \qquad (7)$$

wherein the authors restricted γ to the range $0.1 \leq \gamma \leq 0.5$.

The three nonlinear models stated in (3), (4), and (6) can be described as variants of (7) with an expanded range of the parameter γ. Eq. (7) is identical to (3) when $\gamma = 0$; identical to (4) when $\gamma = -1$; and is the same as (6) for all values of γ. The coefficient λ that appears in these models will take on different numeric values for each model but will remain a distance constant. Therefore, in subsequent analysis, (7) will be used as the primary nonlinear model with relaxed restrictions on the value of γ.

3. The Experiment

The National Center for Atmospheric Research (NCAR) wind tunnel, shown in Fig. 1, is a small open return tunnel with a cylindrical test section 0.9 m in diameter by 1.5 m long (Pike, 1970). The fan is driven by a 25 hp DC motor with SCR (silicon controlled rectifier) speed control. Smooth, stepless control of tunnel speed is possible from below typical anemometer starting speeds to 30 m sec^{-1}. This can be accomplished manually or by a 0 - 5 ma control current. The latter is used for selection of predetermined speeds through a calibrated speed sensor and servo control. The speed sensor is a helicoid propeller anemometer, R. M. Young #27100, with tachometer generator output. Precision switch selectable reference voltages are established in the control circuitry representing 15 speed steps. The sensor and reference voltages feed a high gain operational amplifier which drives a current generator to satisfy the SCR controller requirements.

Since the tunnel is designed to accept a 0 - 5 ma signal to provide continuous speed control, it is possible to disconnect the control circuit and control the tunnel speed with an external signal. This signal can be time-variant to provide a controlled, periodic wind speed in the tunnel. The dynamics of the tunnel flow, the motor and the SCR controller are such that the tunnel speed can be made to increase more rapidly than to decrease. Thus, it would be difficult to produce a simple, periodic speed fluctuation, e.g., a sine wave. Furthermore, the rather slowly decaying speed would severely limit the amplitude-frequency product of the speed.

To simplify data analysis, the tunnel speed should be periodic. To be sensitive to anemometer nonlinear characteristics, the test should stimulate the anemometer with relatively high frequencies. If the fundamental frequency of the input is too low, it will be difficult to detect deviations from anticipated linear response because the anemometer will be able to closely follow the input. If, on the other hand, the fundamental frequency is too high, the anemometer response will be sharply attenuated and difficult to measure accurately. The ideal fundamental test frequency would be close to the anemometer -3dB point from the linear model. However, the anemometer dynamic performance is a function of the mean wind speed so it would be necessary to control frequency and average speed together. The response characteristics of the tunnel were not well known so it was not possible to predict appropriate control signals. Also, the nature of the tunnel control system is such that it is desirable to use an on/off control signal. Thus, a signal generator which produced the waveform shown in Fig. 2 was used. The ON amplitude, period and duty cycle were variable. The period and duty cycle were set experimentally and thereafter, during the test runs, only the amplitude was varied.

Fig. 3 shows the data recording and playback configuration. Three anemometers were used simultaneously in the tunnel. Anemometer S, box 1, was a standard propeller anemometer with four polystyrene blades and tachometer generator output. Anemometer W, box 2, was similar except that each blade was loaded with lead shot to double the moment of inertia.

Anemometer H of box 3 and 5 was a constant temperature hot-film anemometer (Thermo-Systems Inc. Model 1053B with a 1330-60-6 probe) on loan from the Atmospheric Sciences Laboratory, White Sands Missile Range. This anemometer was used to monitor the tunnel speed; however, it was uncalibrated and did not have a linearizing module.

The signals were amplified, box 4, and recorded on a SONY PFM-15 four channel tape recorder, box 6. The data were digitized using the Meteorology Department Metsystem which includes boxes 7 through 10. The data were filtered before digitizing and the sample rate was 10 sec^{-1}. The filter is a second-order active system with a transfer function

$$H(f) = [1 - (f/f_n)^2 + j1.4f/f_n]^{-\frac{1}{2}} \qquad (8)$$

where

f = input frequency

f_n = 14 Hz

The recording procedure was designed to facilitate throughput calibration, that is from the wind tunnel through the complete data path shown in Fig. 3, to the computer.

One of the objectives of the experiment was to demonstrate overestimation of the mean. This requires compensation for the gain and bias contributions of each of the system elements in the data path. The procedure consisted of recording accurately monitored reference voltages, anemometer signals with the tunnel stopped, and anemometer signals when the tunnel speed was slowly increased from zero speed to the maximum used in subsequent tests. The rate of change was slow enough that anemometer lag was insignificant.

4. Preliminary Data Processing

The objectives of preliminary data processing were to (a) digitize the data; (b) perform throughput calibration and linearization of the hot-film anemometer data; and (c) perform Fourier analysis.

(a) Digitization. The data were digitized using the Metsystem which includes an analog input system comprising 14 channels of variable gain (1 to 10) differential amplifiers and second-order, low-pass filters with switch selected bandwidth of 14 Hz to 220 Hz. There is also a 16-channel multiplexer and a 10-bit successive approximation analog-to-digital converter. The three data signals were digitized in parallel at 10 samples sec^{-1} using the filter breakpoints set to 14 Hz.

(b) Throughput Calibration. Anemometer W had been calibrated prior to and after use. From recorded voltage reference signals it is possible to establish the throughput calibration for this anemometer. Since it was most important to insure correspondence between instruments, i.e., relative rather than absolute calibration, the other anemometers were fitted to anemometer W using least squares polynomial regression. Anemometer S was fitted to W using a first-order polynomial to compensate for the composite system gain and bias. The hot-film anemometer H was fitted to W using a fifth-order polynomial to accomplish simultaneous relative calibration and linearization. The data for this matching were obtained by very slowly increasing the tunnel speed from zero to the maximum used in subsequent tests. The data below the threshold region of the propeller anemometers were not used in order to avoid the threshold nonlinearity.

(c) Fourier Analysis. The data were found to be periodic with a period of 8.5 sec corresponding to 85 data points per fundamental cycle. Therefore, it was appropriate to perform Fourier analysis over 85 point segments. The coefficients were averaged over 13 consecutive segments to remove noise. This resulted in 42 amplitude and 42 phase coefficients for each anemometer for each run. However, it was determined, very conservatively, that only the first 19 sets of coefficients need be saved. The amplitude and phase coefficients were corrected to compensate for the system filter whose transfer function was given in (8).

Figs. 4, 6, and 8 show the first 10 amplitude coefficients for anemometers H, S, and W for 3 selected runs of some 25 available. These plots show amplitude on a log scale versus wave number on a linear scale. Wave number was used for convenience since wave number 1 corresponds to a frequency of 1/8.5 sec = 0.118 Hz. There are five lines shown for each wave number. The first is the amplitude for anemometer H. The next two are for anemometer S and the last two are for anemometer W. The first line of each pair is the observed amplitude and the second is the amplitude predicted by linear theory using the corresponding H amplitude as input. From (1) it can be shown that, for a sinusoidal input, the output will be

$$A_p(n) = A_H(n)\left[1 + (\tau\omega)^2\right]^{-\frac{1}{2}} \tag{9}$$

where $A_p(n)$ = amplitude predicted for wave number n for input $A_H(n)$, and τ = time constant = distance constant, λ, divided by the average speed of anemometer H, and ω is the input frequency, $\omega = 2\pi n/8.5$ sec. The distance constants were determined in an earlier step function wind tunnel test described in Appendix B. The distance constant of the standard propeller, S, was 0.98 m while that of the weighted propeller, W, was 1.88 m. These were determined by fitting the data to the linear model.

The two short vertical bars at the top of the graph show the location of the breakpoints for anemometers S and W, again according to linear analysis. The breakpoint frequency is where $\tau\omega = 1$ and is used here to show the relative location of the excitation frequencies.

Figs. 5, 7, and 9 show the data reconstruced from the averaged Fourier coefficients corresponding to Figs. 4, 6, and 8 respectively. In Figs. 5, 7, and 9 the mean and variance are tabulated for each anemometer. The variance of anemometers S and W is less than for H since the propeller anemometers are attenuating frequencies passed by the hot-film anemometer. However, the mean values of S and W are greater than for H. This is the overestimation of the mean predicted by nonlinear models but not by linear models. Since this effect shows up in each run it appears to be a conclusive experimental demonstration of overestimation of the mean.

5. Numerical Analysis.

The objective of the numerical analysis was to determine optimum values for the two parameters, γ and λ, in model (7). To accomplish this, (7) was integrated to produce a predicted output, V_p, which could be compared to the observed propeller anemometer output, V_o.

a. Reconstruction of the data

The numerical integration requires an input stream of data and the optimization process requires a set of comparison data to evaluate the model output. Each data stream was reconstructed from the averaged Fourier coefficients for one complete cycle and can be lengthened indefinitely by simply repeating the cycle. The input data, V_i, is from the hot-film anemometer while the observed output data, V_o, is from one of the two propeller anemometers.

b. Integration

The model (7) was integrated using V_i as the input with interpolation between adjacent points as necessary. The integration procedure requires an initial condition for the output, V_p. The initial value of V_p was set equal to the first point of the observed data, V_o. This could cause a small initial transient which would die out quickly. Therefore the model was integrated over two cycles and only the second cycle was used. This was probably an excessive precaution because the initial transient must have been quite small. The longer the solution runs, the greater the accumulated round-off error. This was controlled by using a fourth-order Runge-Kutta-Gill algorithm with the Thompson (1970) modification. This procedure controls round-off error exceedingly well even on machines with a relatively short word length of 32 bits. The residual error was defined as the difference between the predicted and the observed data, $e = V_o - V_p$, and the error variance σ_e^2 was calculated over the second cycle of the data.

c. Optimization

Initial values of the two model parameters γ and λ were supplied for the integration process. The resulting value of the error variance was used to guide an optimizing routine in selecting new values of γ and λ. Range limits were put on these parameters to allow effective real time graphic display of the optimizing process. The constraints were carefully chosen wide enough to avoid impeding the optimizing process. Therefore the optimizing algorithm was allowed to seek an optimum γ and λ wherever it chose. It was pointed out above that allowing γ to take on an extended range of values made (7) general enough to cover virtually all of the proposed models, thus effectively allowing the optimizing algorithm to choose among these models. The optimizing algorithm is discussed in Appendix C.

d. Results

The analysis process described above was employed on 52 sets of data. Some of these had to be rejected because of clearly identified experimental problems such as failure of the hot-film anemometer. The results were further sorted to simplify presentation. Only eight cases are shown graphically in Figs. 10 through 17, while a total of 32 are summarized in Tables 1 and 2.

Fig. 10 shows the results of fitting the model to the weighted propeller, W, in one case. The input V_i and the observed output for W, V_o, are plotted in the top portion while the error $e = V_o - V_p$, magnified 7.6 times, is plotted in the lower portion. The units of e are m sec^{-1}. The predicted output, V_p, is not shown in the top portion because it would lie so close to V_o. In some examples, most notably Fig. 15, the error curve lies wholly above the zero line indicating a residual bias. This shows that the model did not completely predict the full amount of the overrun in the observed data.

Table 1 summarizes the analyzed data. The column headings are explained below:

Col. 1. Data grouping by average tunnel speed class.

Col. 2. $\overline{V}_H$ = average hot-film anemometer speed.

Col. 3. σ_H^2 = variance of hot-film anemometer.

Col. 4. Type designation is O for observed data, N for data output of the nonlinear model, and L for results of the linear model.

Table 1. Summary of analysis of 32 sets of data.

1	2	3	4	Standard Propeller Anemometer S 5	6	7	8	Weighted Propeller Anemometer W 9	10	11	12
Class	$\overline{V}_H$ m sec^{-1}	σ_H^2 m^2 sec^{-2}	Type	$\overline{V}_S$ m sec^{-1}	σ_S^2 m^2 sec^{-2}	Over-run %	VR %	$\overline{V}_W$ m sec^{-1}	σ_W^2 m^2 sec^{-2}	Over-run %	VR %
1	1.57	.420	O	1.62	.322	2.8	76.7	1.65	.206	5.2	48.7
			N	1.60	.316	2.1	75.3	1.64	.203	4.8	48.4
			L	1.57	.343	0	83.1	1.57	.232	0	57.2
2	1.68	.419	O	1.74	.329	3.4	78.5	1.78	.212	5.6	50.6
			N	1.71	.323	1.8	77.1	1.75	.211	4.3	50.3
			L	1.68	.348	0	83.1	1.68	.240	0	57.2
3	2.81	.922	O	2.85	.825	1.6	89.4	2.89	.643	2.9	69.7
			N	2.85	.808	0.6	87.7	2.88	.633	2.3	69.5
			L	2.81	.832	0	90.3	2.81	.687	0	74.5
4	3.39	1.14	O	3.44	1.05	1.5	92.2	3.47	.855	2.6	75.2
			N	3.39	1.03	0.2	90.7	3.44	.847	1.6	74.5
			L	3.39	1.05	0	92.2	3.39	.902	0	79.3

Table 2. Summary of parameter optimization on 32 sets of data.

		S			W		
		Non-linear		Linear	Non-linear		Linear
Class	$\overline{V}_H$ m sec^{-1}	γ	λ m	λ m	γ	λ m	λ m
1	1.57	-.95	1.71	.836	-.76	3.25	1.71
2	1.68	-.76	1.58	.848	-.62	3.09	1.75
3	2.81	-1.38	2.18	.887	-.48	2.93	1.76
4	3.39	-3.61	4.28	.890	-.64	3.63	1.76

Col. 5 and 9. Mean speed observed or predicted.

Col. 6 and 10. Variance observed or predicted.

Col. 7 and 11. Observed overrun percentage, $100(\overline{V}_s - \overline{V}_H)/\overline{V}_H$.

Col. 8 and 12. Percentage of input variance observed in the propeller anemometer, $100\ \sigma_s^2/\sigma_H^2$.

The hot-film anemometer output is taken to be a good measure of the tunnel speed. The first two columns of Table 1 show the average and variance of the tunnel speed. Variance is used as a measure of the speed fluctuation since the speed was composed of many frequency components. Columns 5, 6, 9 and 10, line O show that the propeller anemometer consistently overestimated the mean and reduced the variance. Columns 7 and 11 show the overrun percentage, the amount by which the output mean exceeded the input. Columns 8 and 12 show output variance as a percentage of the input variance.

The results of the nonlinear model are shown on line N. The model consistently overestimates the mean although less than observed in the anemometer. The model also consistently underestimates the output variance.

The linear model (1) with $\tau = \lambda\overline{V}_i^{-1}$ was run for comparison purposes. Even though it has only one parameter, λ, the same optimizing routine was used. The results are shown on line L and indicate no overrun and the model variance is consistently higher than the observed output.

The optimized parameters are shown in Table 2 for both propeller anemometers and for both the linear and the nonlinear models. The dimensionless parameter γ showed considerable fluctuation but was consistently negative. The parameter λ has a trend in the higher speed classes for anemometer S that is not as pronounced for anemometer W. The distance constants for the linear model are low compared to the results previously obtained from step function wind tunnel testing. Those results were $\lambda = 0.98$ m for anemometer S and $\lambda = 1.88$ m for W.

6. Interpretation.

a. Model fitting

In Table 1 the overestimation of the mean decreases with increasing wind speed and the output-to-input variance ratio increases. This can be explained, using the linear model as a guide, by noting that the time constant τ is an inverse function of the wind speed. Thus one would expect the anemometer performance to improve as the mean wind speed increases provided that the input signal does not shift to higher frequencies in the same way. Comparing Figs. 4 and 8, it can be seen that while the input variance has more than doubled (see Table 1), the distribution of the input variance has not shifted markedly. There is, however, the expected improvement in the distribution of the observed anemometer variance. Also, the standard propeller, S, performs better than the weighted propeller which fits the general pattern of results.

The linear model is incapable of explaining the overestimation of the mean since in (1) the steady-state average output must equal the average input. The linear variance ratio, columns 8 and 12, approaches the observed variance ratio as the average speed increases. Evidently the nonlinear characteristics of the propellers are a function of the mean wind speed given that the variance distribution does not change much. This too could be expected since as the speed increases and the anemometer performance improves, the input variance occurs mainly at frequencies below the anemometer -3 dB point. Figs. 4 and 8 show that there is relatively little attenuation or nonlinear distortion at frequencies up to the -3 dB point.

The nonlinear model seems to fit best when there is considerable nonlinear distortion. The more overrun in the observed data, the better the nonlinear model explains it. In Table 1, when the overrun is 5.2% the model result is 4.8% but when the observed overrun drops to 1.5% the model result is only 0.2%. The model also fits the variance ratio best when it is lowest (indicating greater anemometer attenuation), and is a somewhat poorer fit when the variance ratio exceeds 90%.

With this background it is easier to interpret the parameter values of Table 2. The values for the nonlinear model, when applied to anemometer S, change markedly with the wind speed. As observed above, the nonlinear model does not fit well when the nonlinear distortion is small and as a consequence the optimizer is forced to shift γ and λ over a large range in its attempt to fit the observed data. These large shifts in parameter values were accompanied by very small changes in the residual error variance. In one case the optimizer moved from $\gamma = -2.16$, $\lambda = 2.86$ to $\gamma = -3.01$, $\lambda = 3.59$ to reduce the residual error variance from $1.11 \times 10^{-4}\ m^2\ sec^{-2}$ to $1.10 \times 10^{-4}\ m^2\ sec^{-2}$. In this case the input variance was $1.14\ m^2\ sec^{-2}$ so a very large change in parameter value was required to produce a trivial improvement in the quality of the fit. On this basis it is reasonable to assign more weight to lines 1 and 2 of Table 2 than to lines 3 and 4.

b. Model interpretation

Eq. (7) can be written in another form,

$$\frac{dV}{dt} = \frac{(V_i - \gamma V)}{\lambda} (V_i - V) \tag{10}$$

and interpreted by comparison with (3), repeated here in the form

$$\frac{dV}{dt} = \frac{V_i}{\lambda} (V_i - V). \tag{3}$$

In (3) λV_i^{-1} represents the time constant and $(V_i - V)$ represents the deviation from equilibrium conditions upon which the anemometer operates. The time constant could not really be equal to λV_i^{-1} because that implies that $\tau = \infty$ when $V_i = 0$ which means that if the anemometer were initially set into motion in still air, it would never stop. The propeller dissipates its overspeed energy into the air stream, and it is reasonable to expect this energy transfer to be a function of both the air speed and of the propeller speed. The simplest function is $\tau = \lambda(V_i + V)^{-1}$ and since γ was observed to be in the range -1.4 to -0.5, the $\lambda(V_i - \gamma V)^{-1}$ term of (10) appears to be a modified time constant.

It was earlier required that the model be linear in the static sense, i.e., that $dV/dt = 0$ when $V = V_i$. Thus γ could not be positive since then $dV/dt = 0$ in (10) when $V = V_i$ and when $\gamma V = V_i$. Even with $\gamma < 0$ (10) is not generally adequate since both V and V_i can go negative for a propeller anemometer. The problem did not arise in the wind tunnel study where $V_i > 0$. Evidently a more general expression would be

$$\frac{dV}{dt} = \frac{(|V_i| - \gamma|V|)}{\lambda}(V_i - V) \tag{11}$$

which always satisfies the static linearity requirement for $\gamma < 0$.

c. Response to a cosine input

It is useful to explore the properties of (11) by using a simple input $V_i = a + b \cos \omega t$ where $a > 0$ and $b \leq a$. In this case (11) is equivalent to (10) or (7).

It is useful to put (10) in dimensionless form. Let

$$\alpha = b/a$$

$$U = V/a$$

$$U_i = V_i/a$$

$$T = \omega t$$

then

$$\frac{dU}{dT} = \frac{1}{\beta}(U_i - \gamma U)(U_i - U) \tag{12}$$

where $\beta = \omega\lambda/a$ and $U_i = 1 + \alpha \cos T$. This reduces the five parameters a, b, ω, γ, λ to three: α, β and γ. The parameter α is a gustiness factor, β is a dimensionless frequency and γ is unchanged. To further simplify the analysis let γ be a constant. The amount of nonlinear distortion is proportional to the "gustiness factor" α so, for maximum effect, let $\alpha = 1$. Figs. 18 through 22 show the solution of (12) as β is increased from 0.10 to 10.0. In each case the input is a cosine wave of unit amplitude and each figure shows one full cycle. In Fig. 18 the top portion of the solution deviates very little from the cosine wave but the lower portion shows some distortion. The input mean value is 1.0 but the output mean value appears to be greater than 1.0. As the frequency (β) increases, the amount of distortion increases, as does the overrun until $\beta = 1$. As β continues to increase, the amount of distortion decreases as the input is attenuated more and more. When $\beta = 10$, there is little evident distortion but considerable overrun. The solution of (12) for $U_i = 1 + \alpha \cos T$ would be of the form

$$\begin{aligned} U(T) = 1 + A_1 &+ A_2\cos(T + \varphi_1) \\ &+ A_3\cos(2T + \varphi_2) \\ &+ A_4\cos(3T + \varphi_3) + \ldots \end{aligned} \tag{13}$$

where A_1, A_2, A_3, A_4, . . . are all functions of α, β and γ. The numerical solutions of (12) were generated and analyzed for $\gamma = -0.652$, $0.05 \leq \alpha \leq 1.00$, and $0.1 \leq \beta \leq 100$. In this range, the maximum overrun of 25% was produced for $\alpha = 1.0$ and $\beta = 8.0$. For all values of α, the maximum overrun occurred for $7 \leq \beta \leq 8$. The -3 dB point is at approximately $\beta = 1.7$.

The maximum first harmonic, the A_3 term, is produced for $\alpha = 1$ and $\beta = 0.9$ with amplitude 0.135. At this point the amplitude of the fundamental is 0.761 so this represents a significant distortion as shown in Fig. 20.

Both maximum overrun and maximum distortion are produced for large values of α, the "gustiness" parameter. For a given α, maximum distortion occurs at relatively low frequencies, $\beta < 1$, while maximum overrun occurs at relatively high frequencies, $\beta > 1$. This affords a useful definition of relative frequency. It is high if $\beta > 1$, low if $\beta < 1$. Table 3 gives the β values for the test conditions for the fundamental tunnel frequency and the first 3 harmonics. This indicates that the propellers in the wind tunnel were operating in the region of maximum distortion but not in the region of maximum overrun. This explains the low values of overrun observed.

Table 3. Values of $\beta = \omega\lambda\overline{V}^{-1}$ (dimensionless) for the test conditions.

Avg. Speed m sec^{-1}	Fundamental	Harmonics 1	Harmonics 2	Harmonics 3
1.57	.47	.94	1.4	1.9
2.81	.26	.53	.79	1.1
3.39	.22	.44	.65	.87

7. Conclusions.

A new test procedure for mechanical anemometers has been devised using a wind tunnel in which the speed can be controlled to produce a periodic flow with sufficient amplitude and the appropriate frequencies to stimulate nonlinear anemometer performance. One measure of nonlinear performance, overrun, was consistently produced.

The experimental procedure and the data analysis procedure described here can be simplified for easier application. Once an analysis program is operating satisfactorily it is possible to quickly change the model to be tested and therefore evaluate a variety of models with ease. This experiment could very well become a new standard test for mechanical anemometers since the tunnel flow is repeatable and reasonably realistic and the data analysis is completely objective. The usual step function wind tunnel test has none of these advantages.

Acknowledgements.

The author is deeply indebted to Professor Claude Duchon for his advice and encouragement.

The Atmospheric Science Laboratory of the White Sands Missile Range provided access to their wind tunnel and the loan of a hot-film anemometer. A part of the computation was done using the CDC 6600 computer at the National Center for Atmospheric Research which is sponsored by the National Science Foundation. NCAR also provided access to their new wind tunnel without which this work could not have been done.

The author also wishes to gratefully acknowledge the assistance of Mrs. Joan A. Jones.

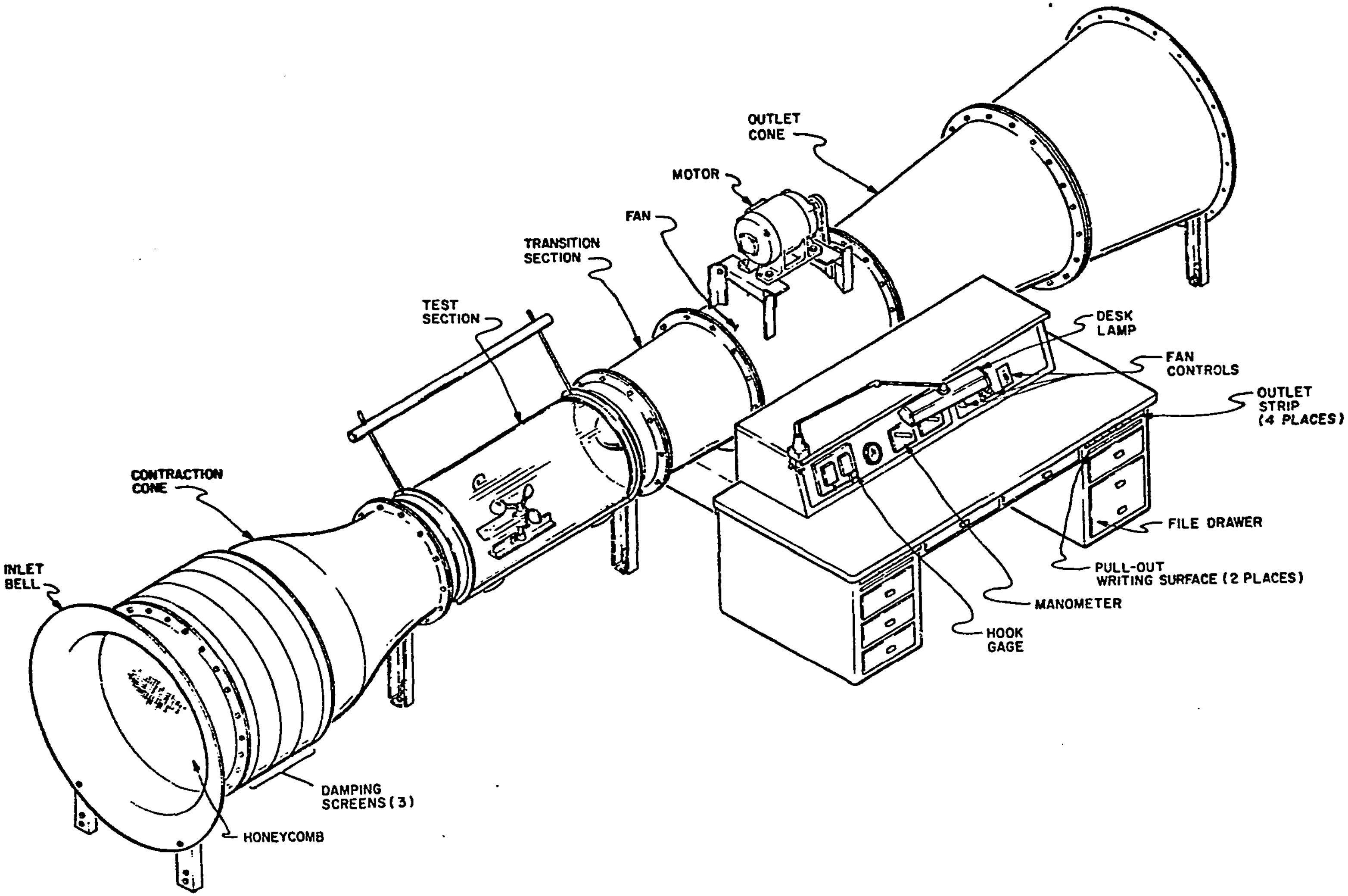

Fig. 1. NCAR wind tunnel.

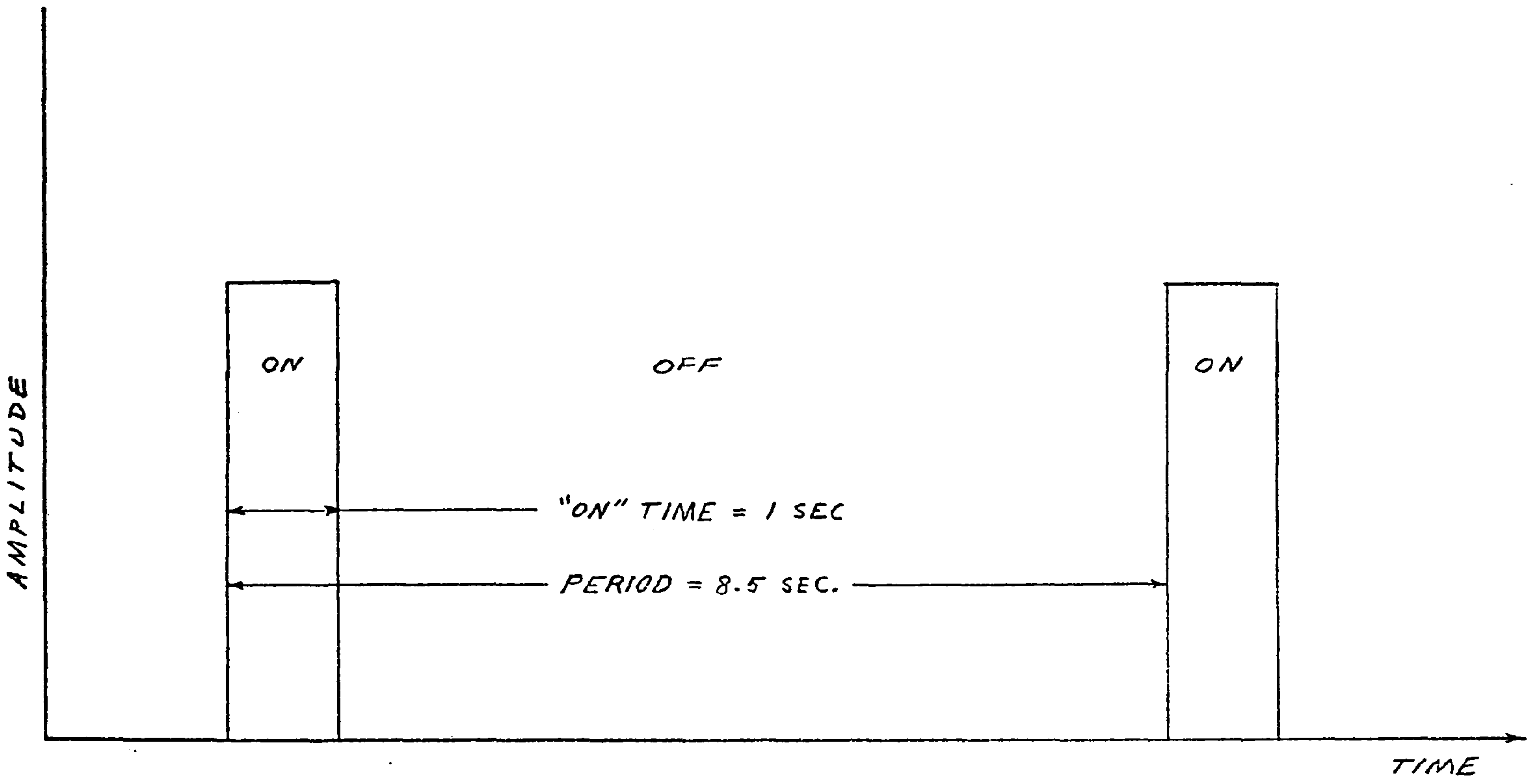

Fig. 2. Special external wind tunnel control signal.

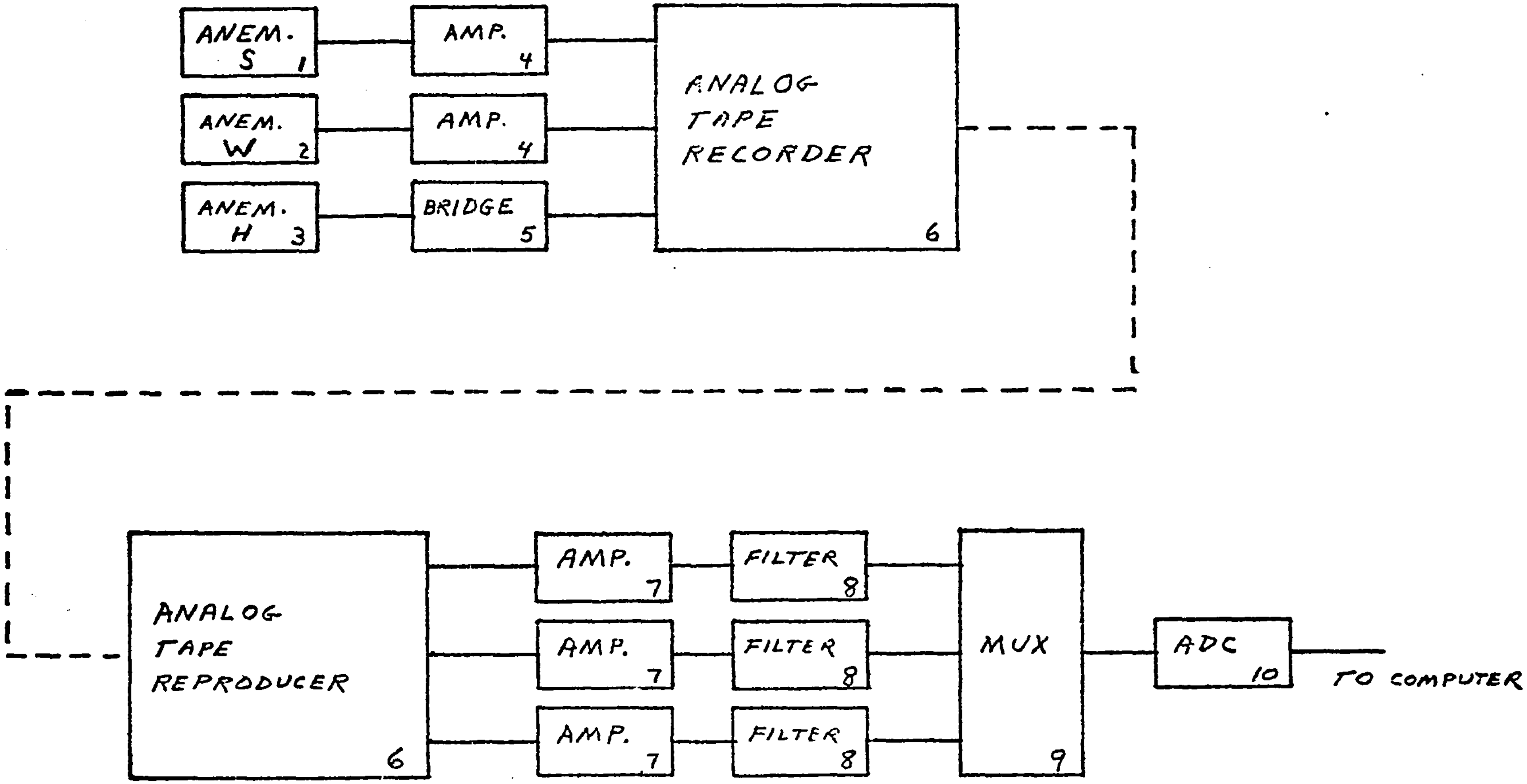

Fig. 3. Data recording and playback configuration.

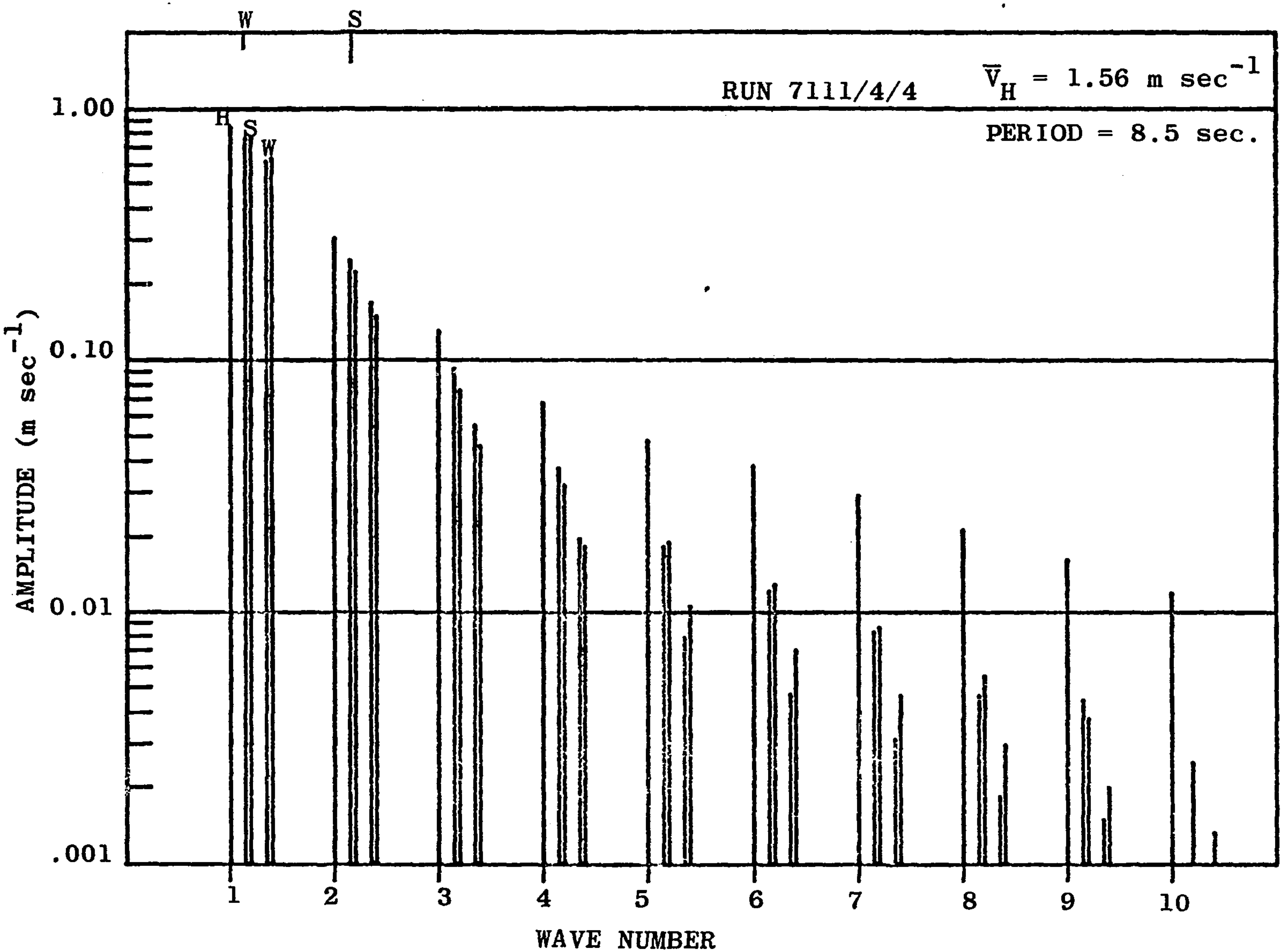

Fig. 4. Averaged Fourier analysis of data.

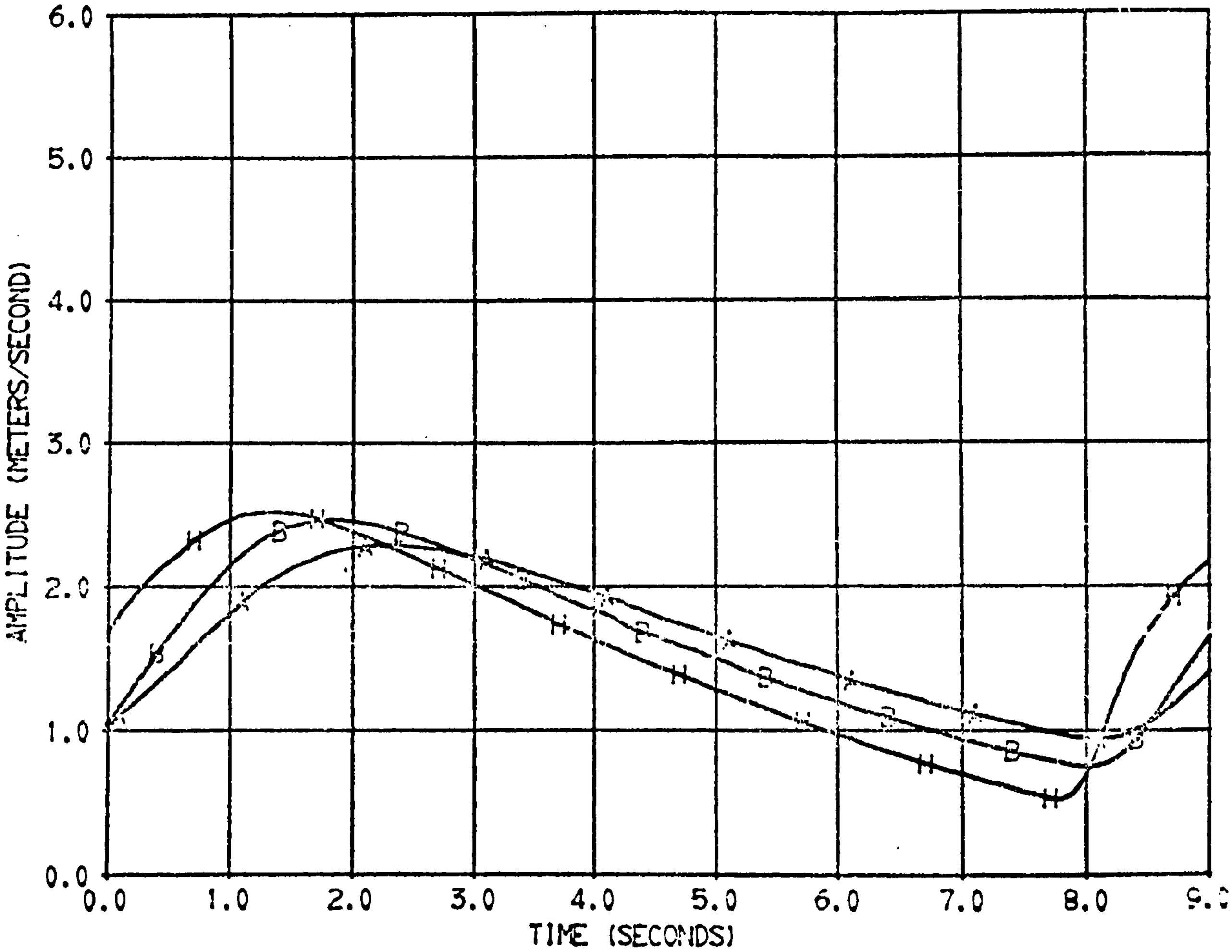

RUN 7111/ 4/4 PERIOD = 8.5 SEC

	W	S	H
MEAN	1.642	1.611	1.563
VARIANCE	.206	.324	.420

Fig. 5. Data reconstructed from averaged Fourier coefficients. Curve labeled A is for propeller anemometer W, B is for propeller S, and H is for the hot-film anemometer.

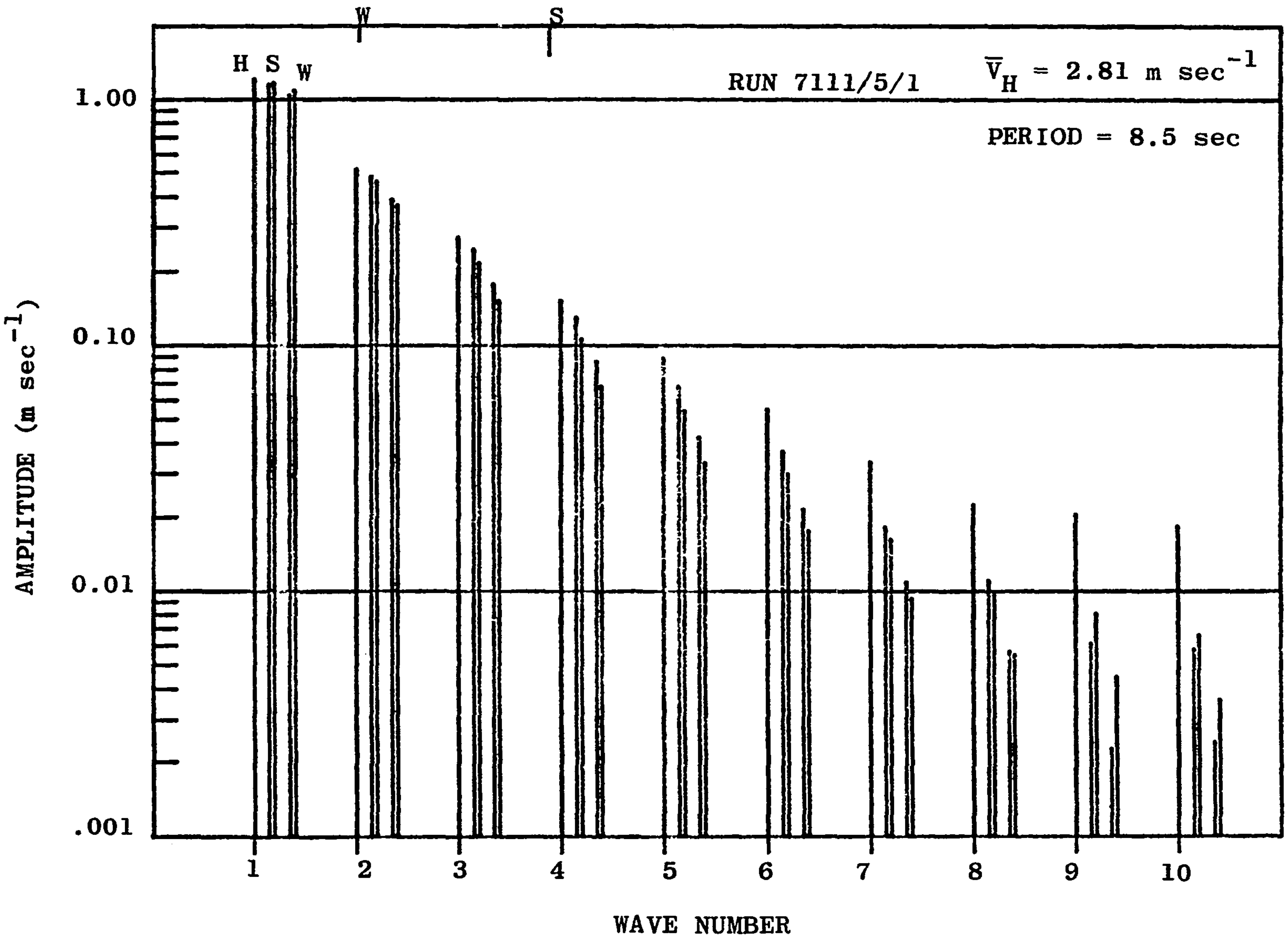

Fig. 6. Averaged Fourier analysis of data.

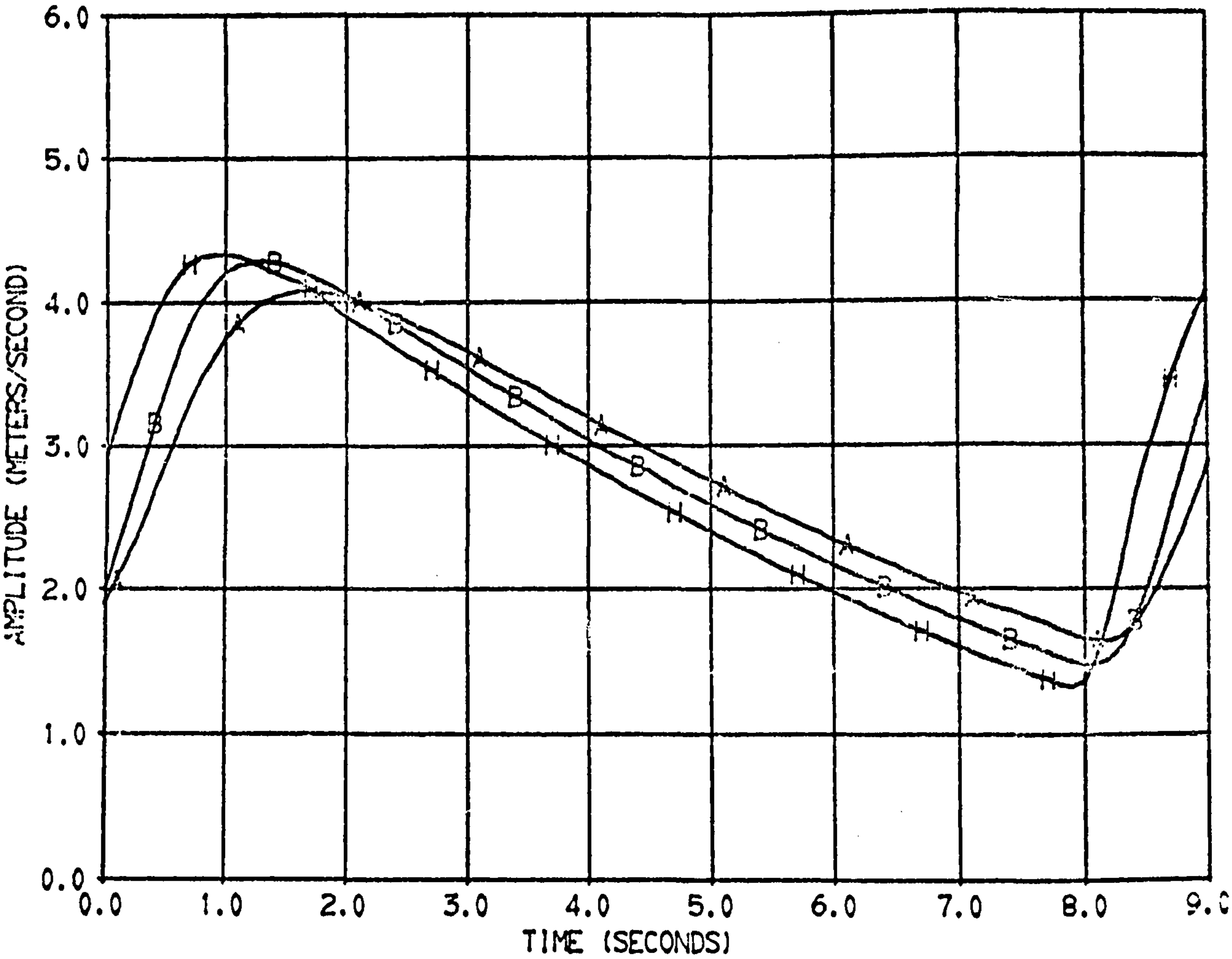

RUN 7111/ 5/1 PERIOD = 8.5 SEC

	W	S	H
MEAN	2.885	2.851	2.812
VARIANCE	.640	.822	.929

Fig. 7. Data reconstructed from averaged Fourier coefficients. Curve labeled A is for propeller anemometer W, B is for propeller S, and H is for the hot-film anemometer.

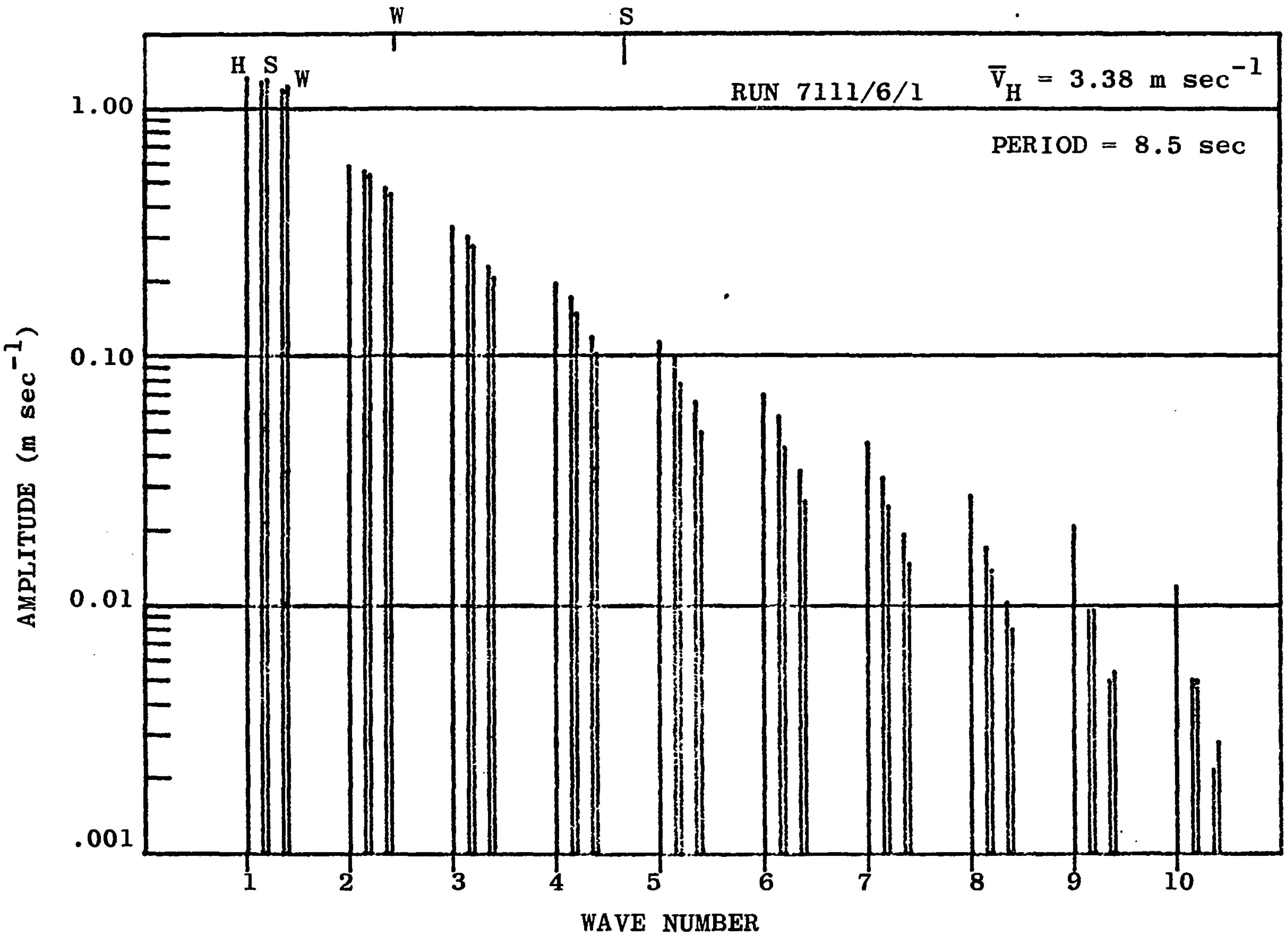

Fig. 8. Averaged Fourier analysis of data.

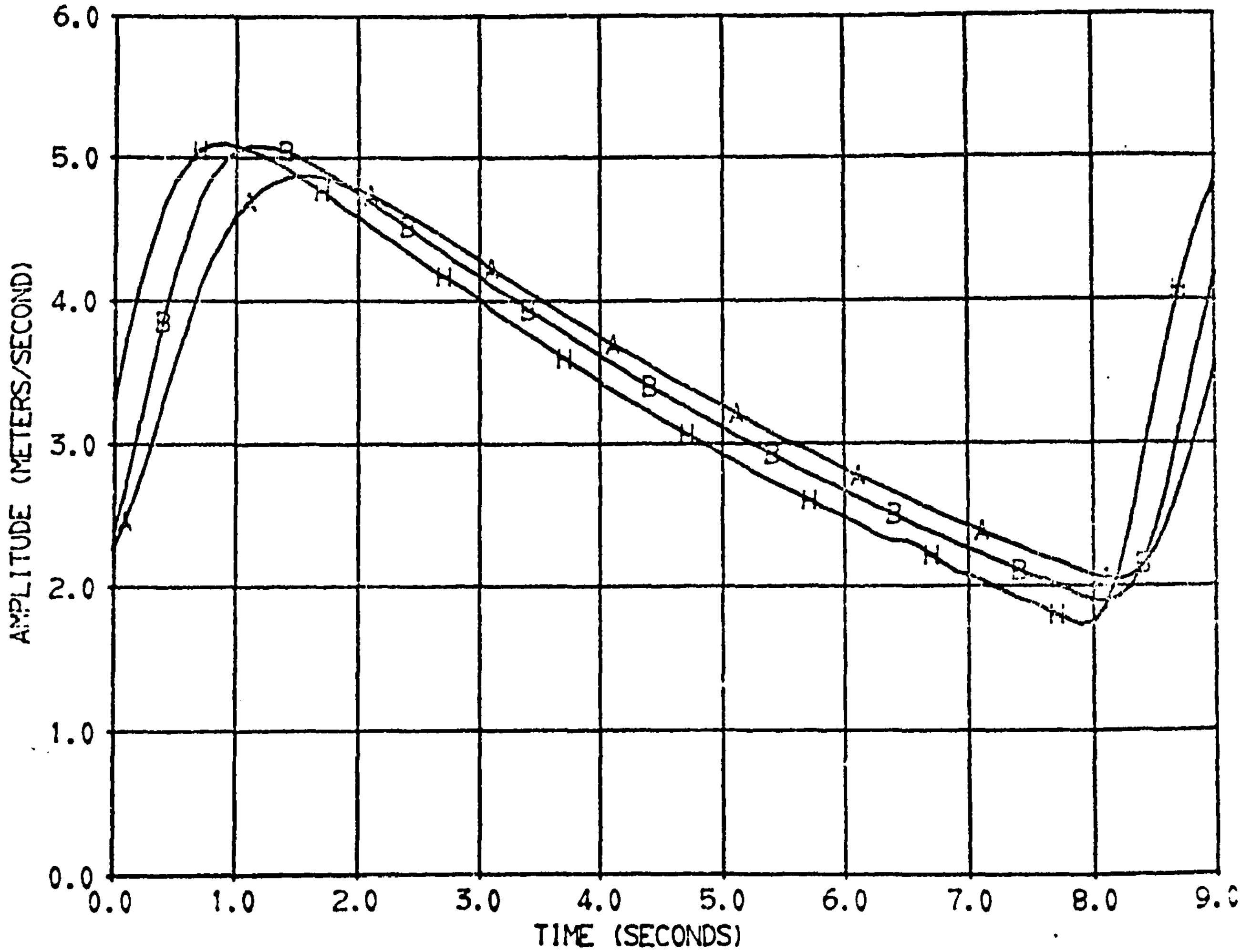

RUN 7111/ 6/1 PERIOD = 8.5 SEC

	W	S	H
MEAN	3.452	3.426	3.375
VARIANCE	.858	1.053	1.147

Fig. 9. Data reconstructed from averaged Fourier coefficients. Curve labeled A is for propeller anemometer W, B is for propeller S, and H is for the hot-film anemometer.

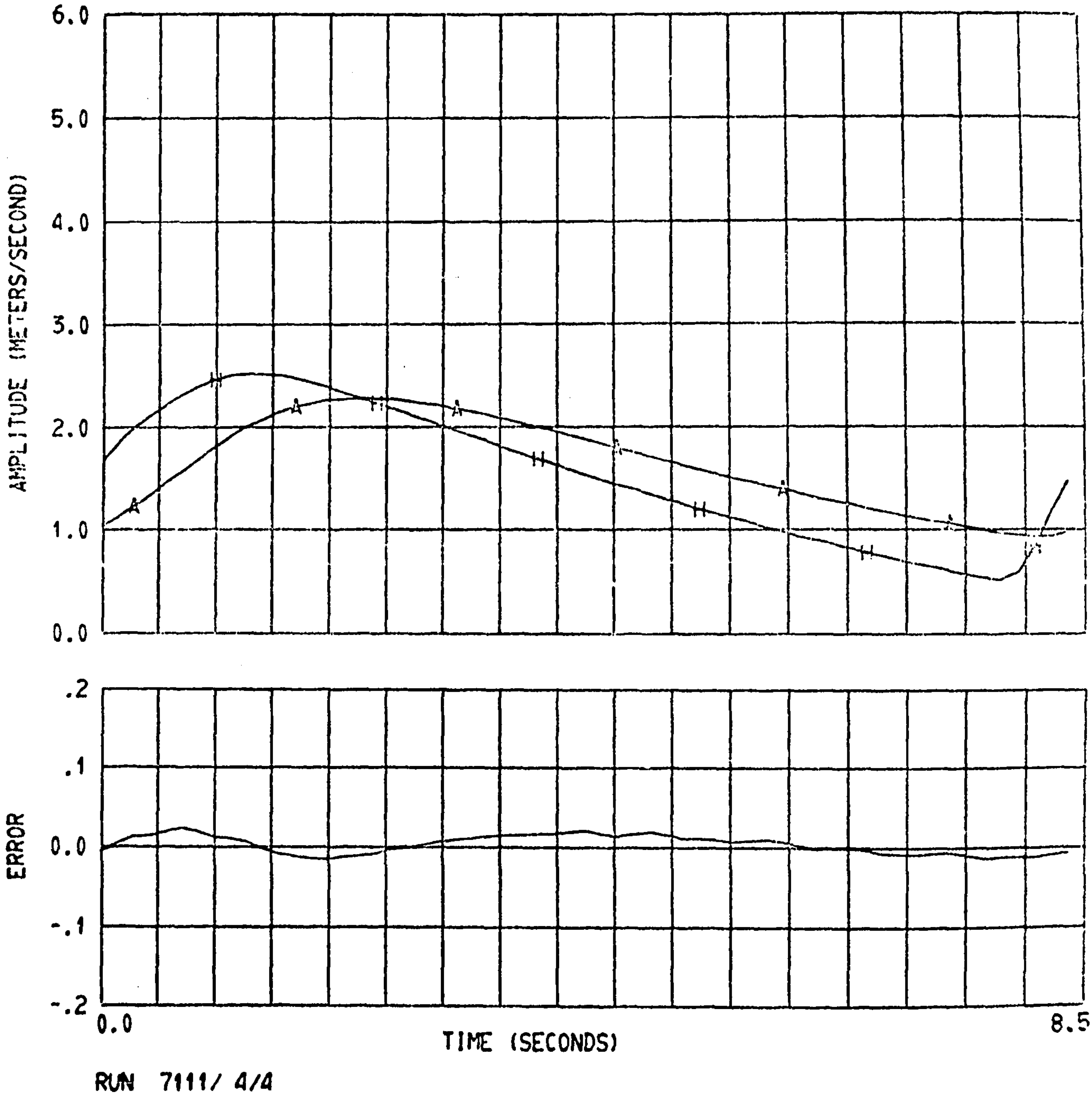

Fig. 10. Results of optimization procedure on anemometer W. The residual error (units = m sec^{-1}) is shown at bottom.

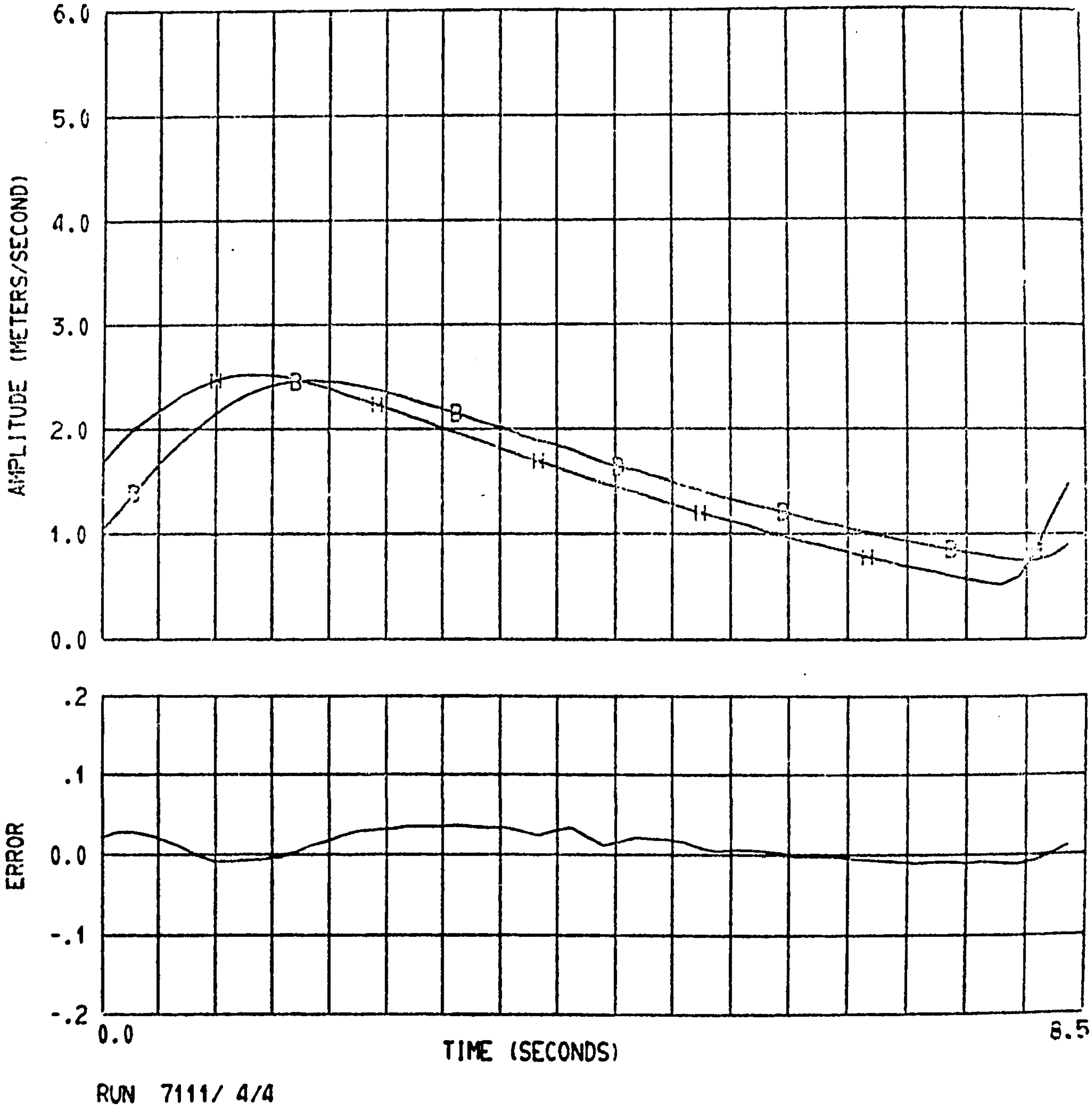

Fig. 11. Results of optimization procedure on anemometer S. The residual error (units = m sec^{-1}) is shown at the bottom.

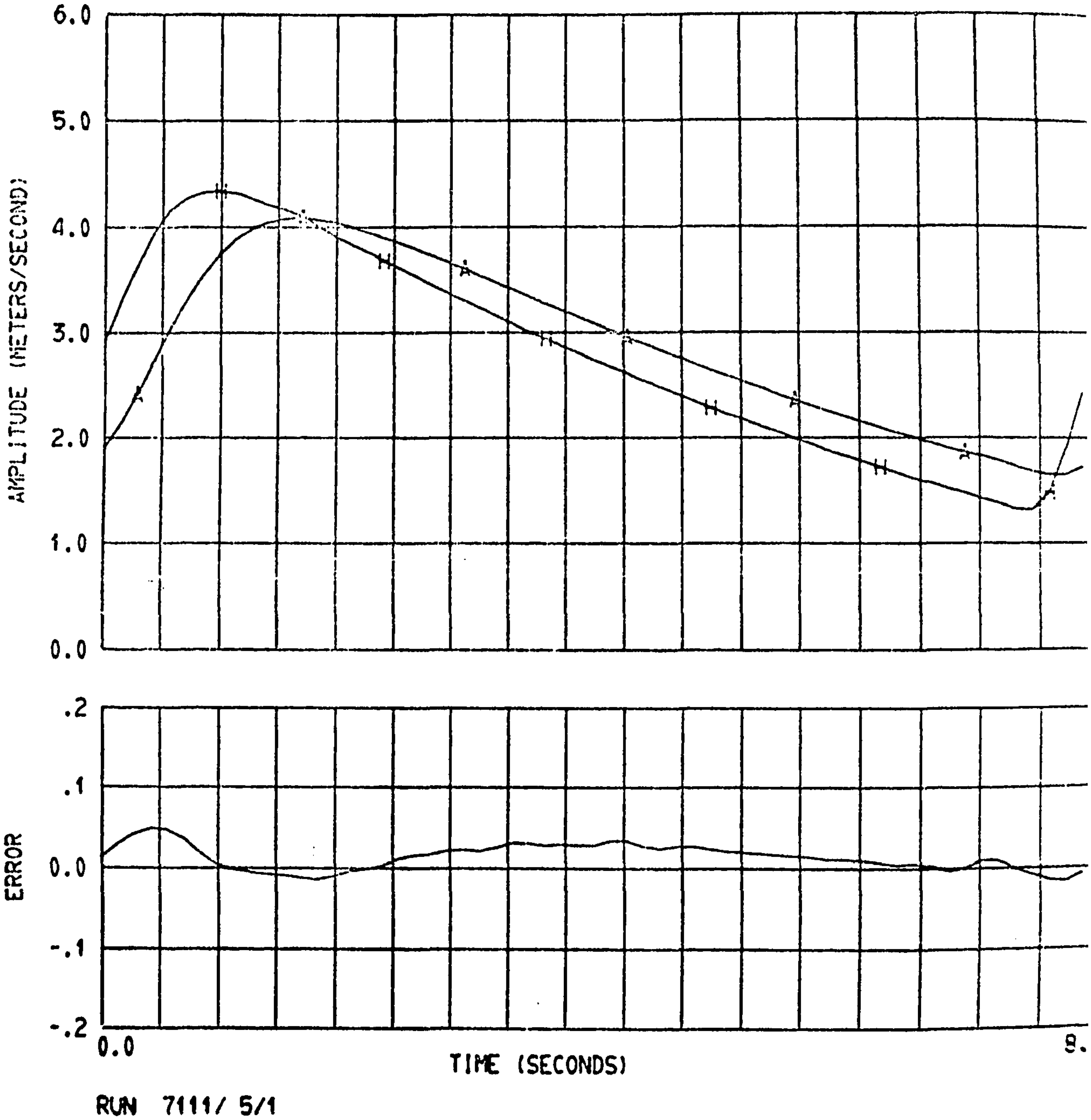

Fig. 12. Results of optimization procedure on anemometer W. The residual error (units = m sec^{-1}) is shown at bottom.

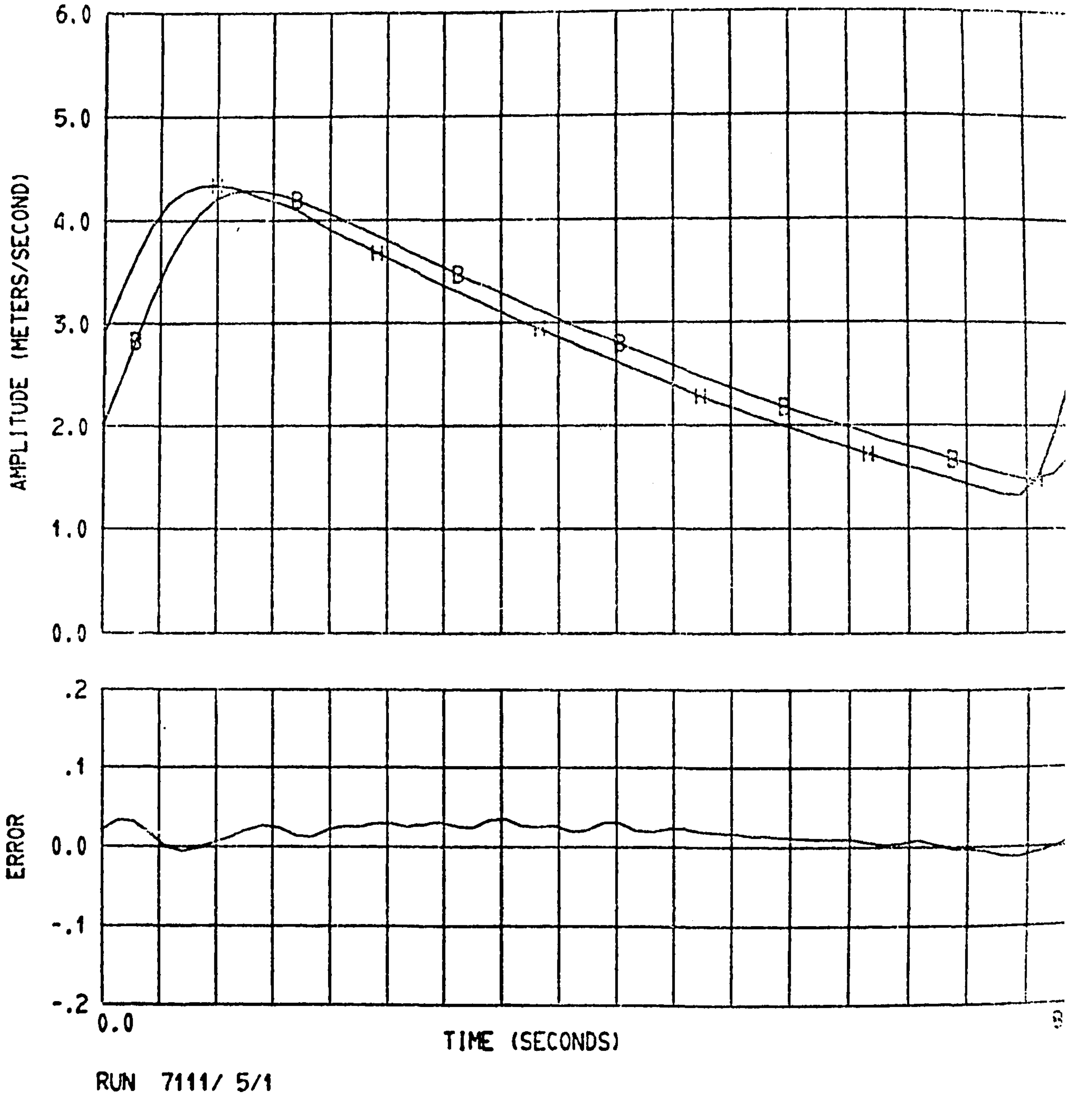

Fig. 13. Results of optimization procedure on anemometer S. The residual error (units = m sec^{-1}) is shown at the bottom.

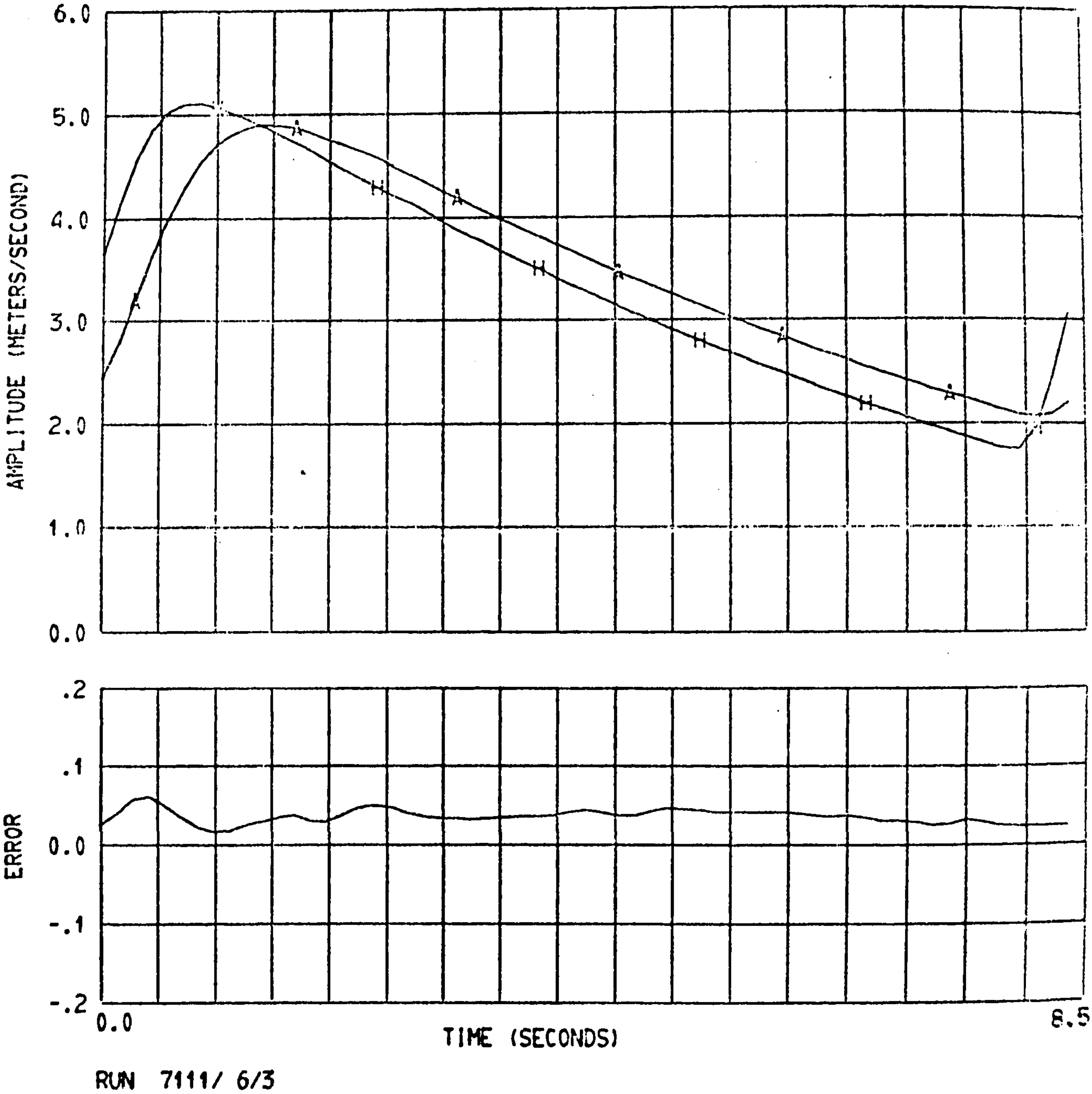

Fig. 14. Results of optimization procedure on anemometer W. The residual error (units = m sec^{-1}) is shown at bottom.

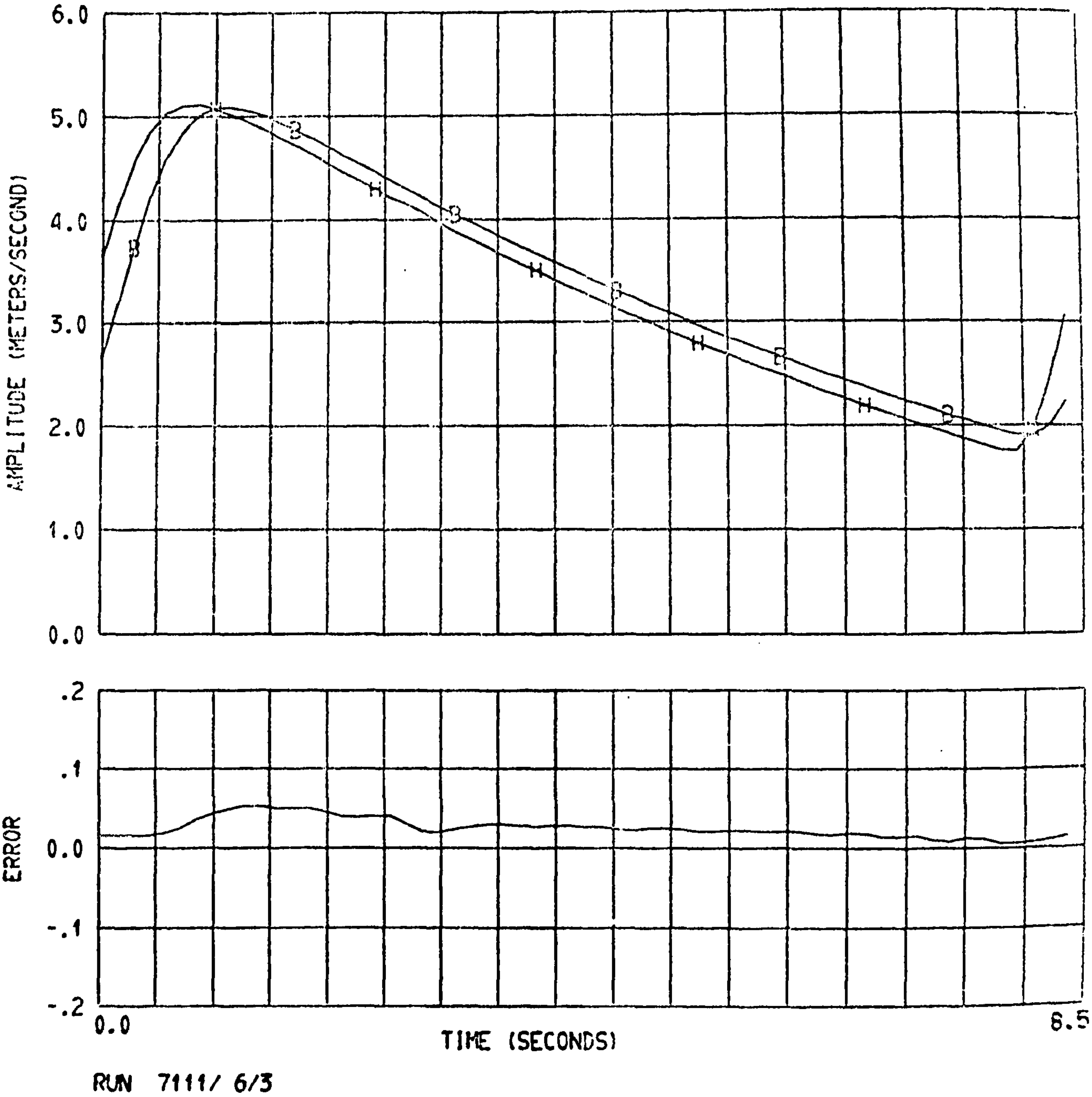

Fig. 15. Results of optimization procedure on anemometer S. The residual error (units = m sec^{-1}) is shown at the bottom.

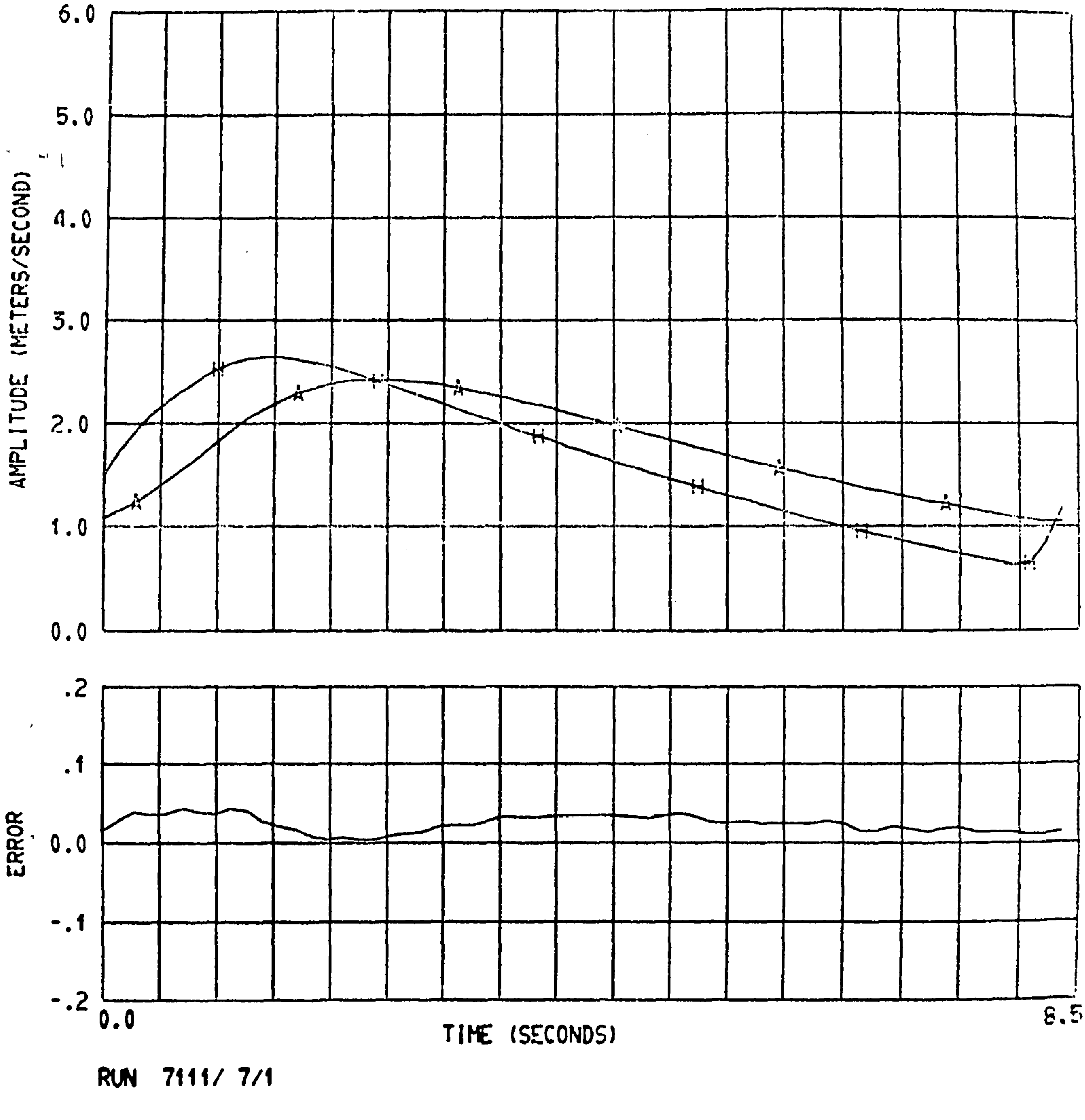

Fig. 16. Results of optimization procedure on anemometer W. The residual error (units = m sec^{-1}) is shown at bottom.

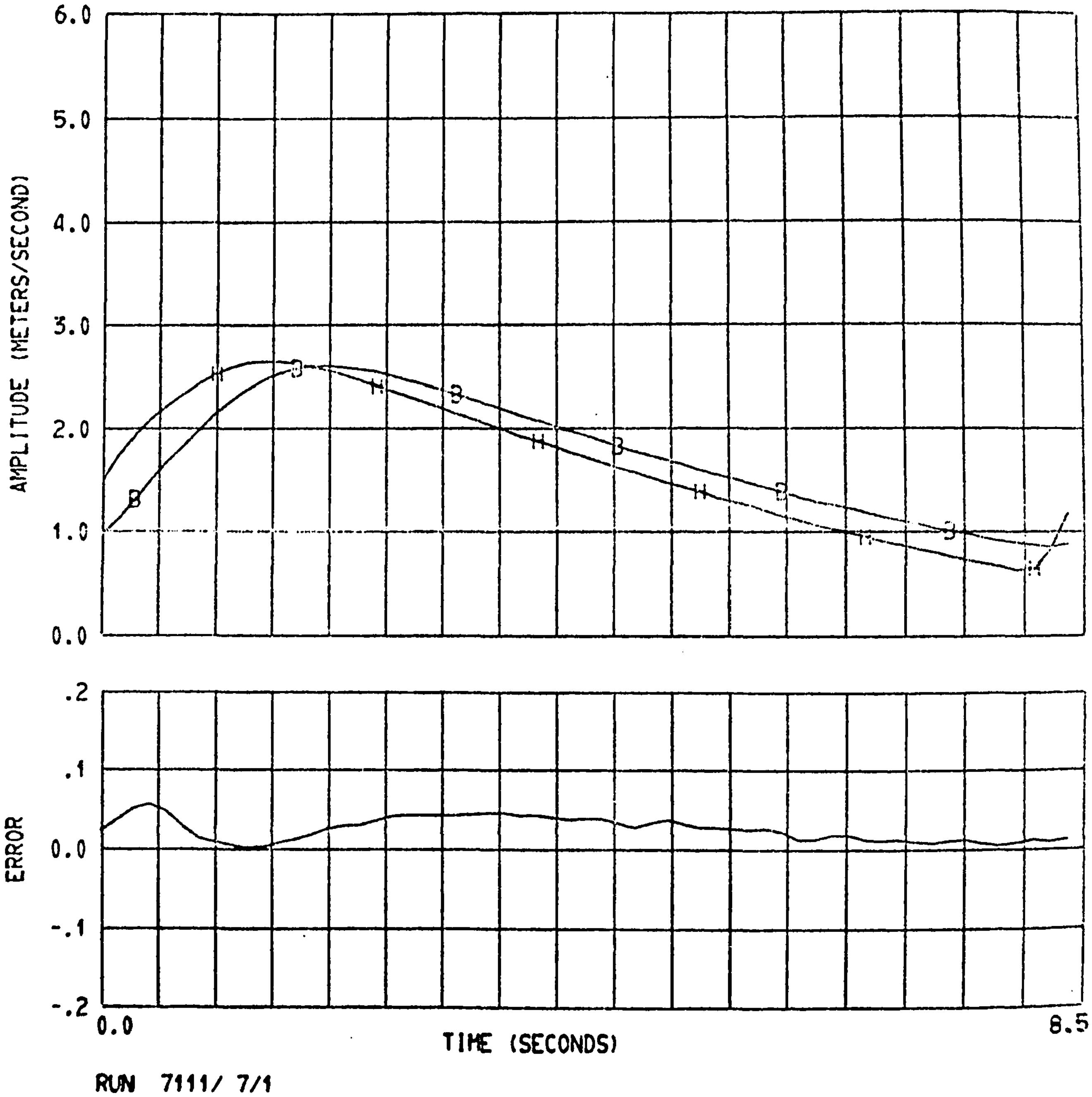

Fig. 17. Results of optimization procedure on anemometer S. The residual error (units = m sec^{-1}) is shown at the bottom.

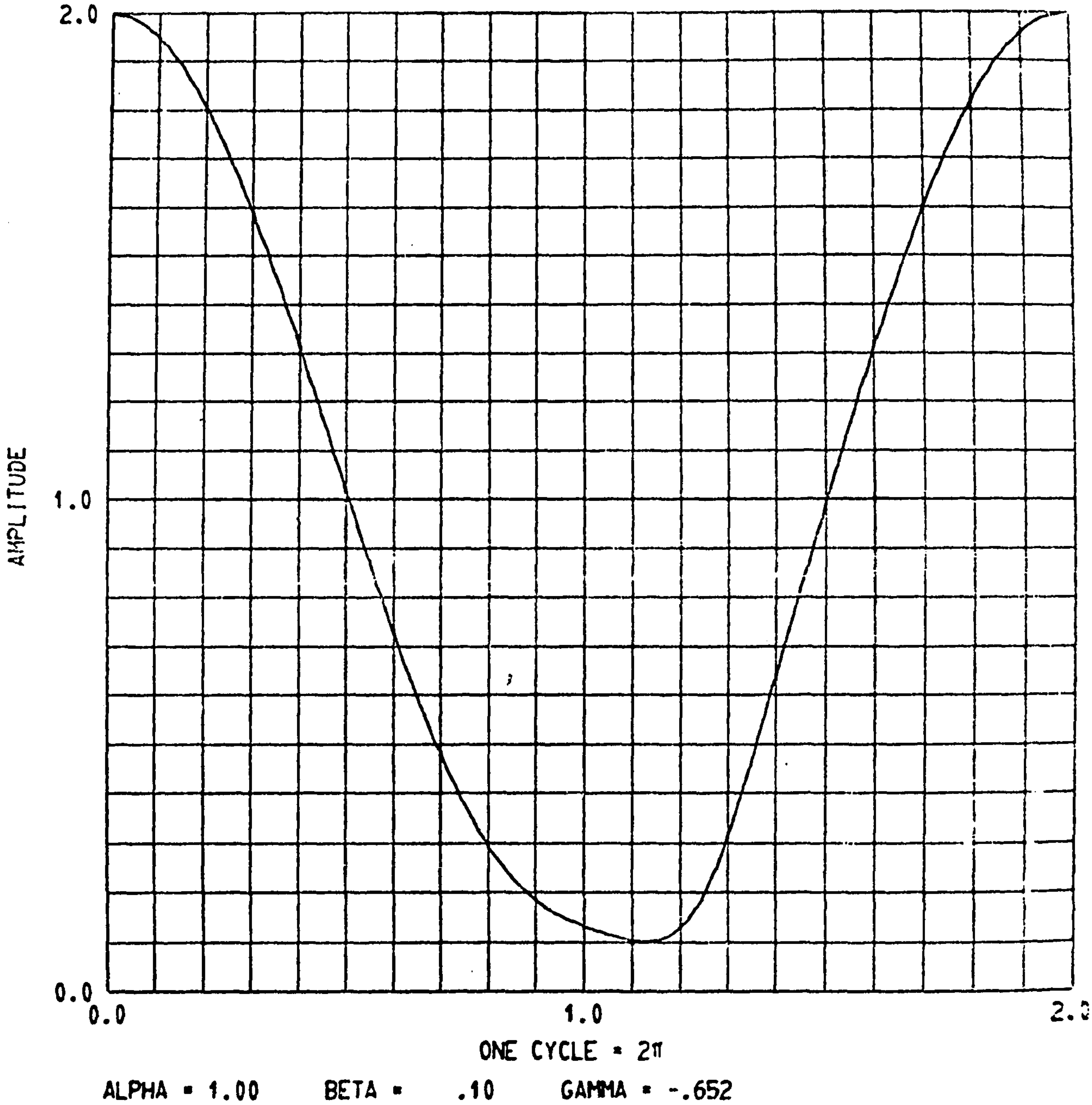

Fig. 18. Output of Eq. (12) when input is a cosine wave.

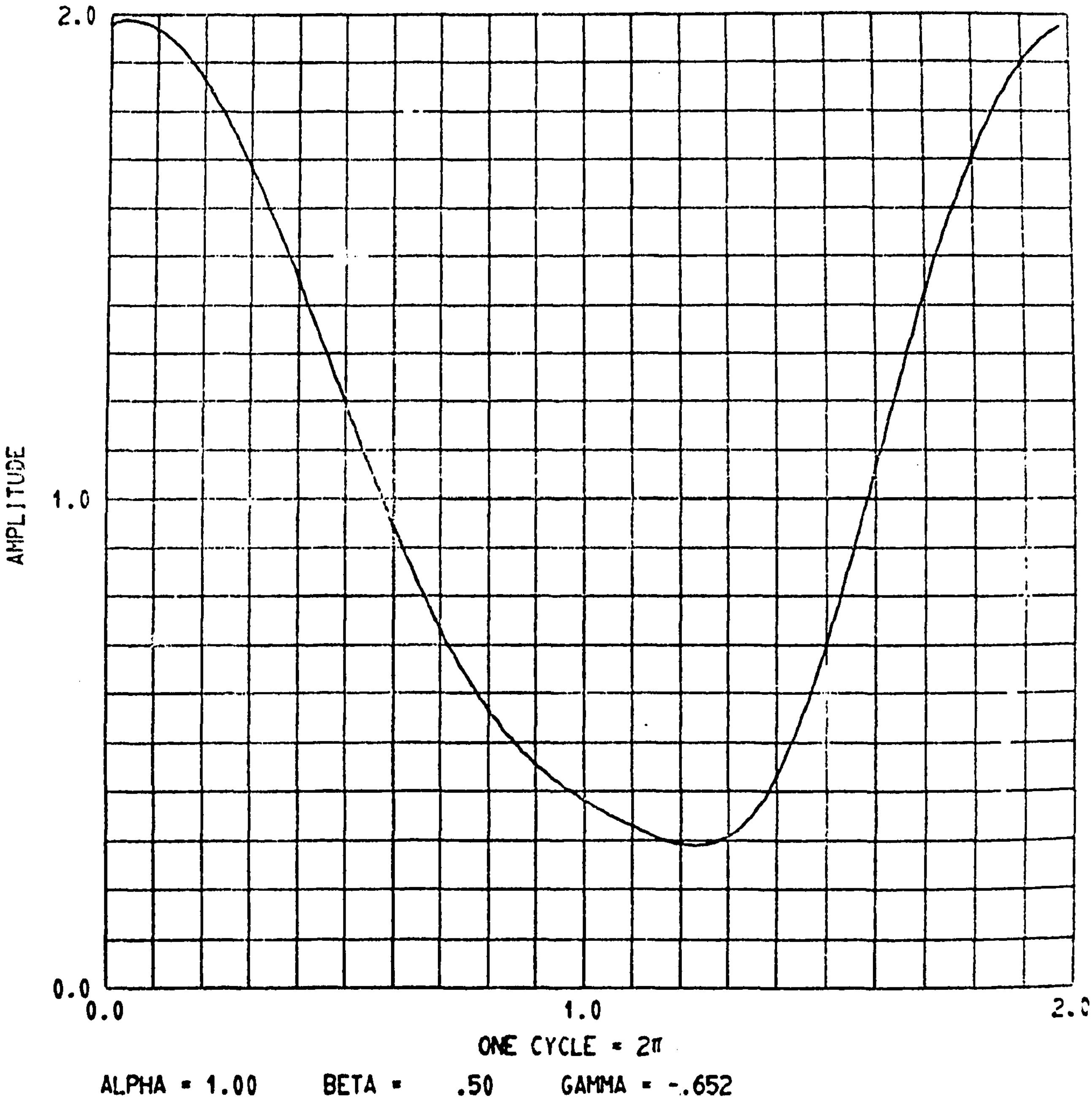

Fig. 19. Output of Eq. (12) when input is a cosine wave.

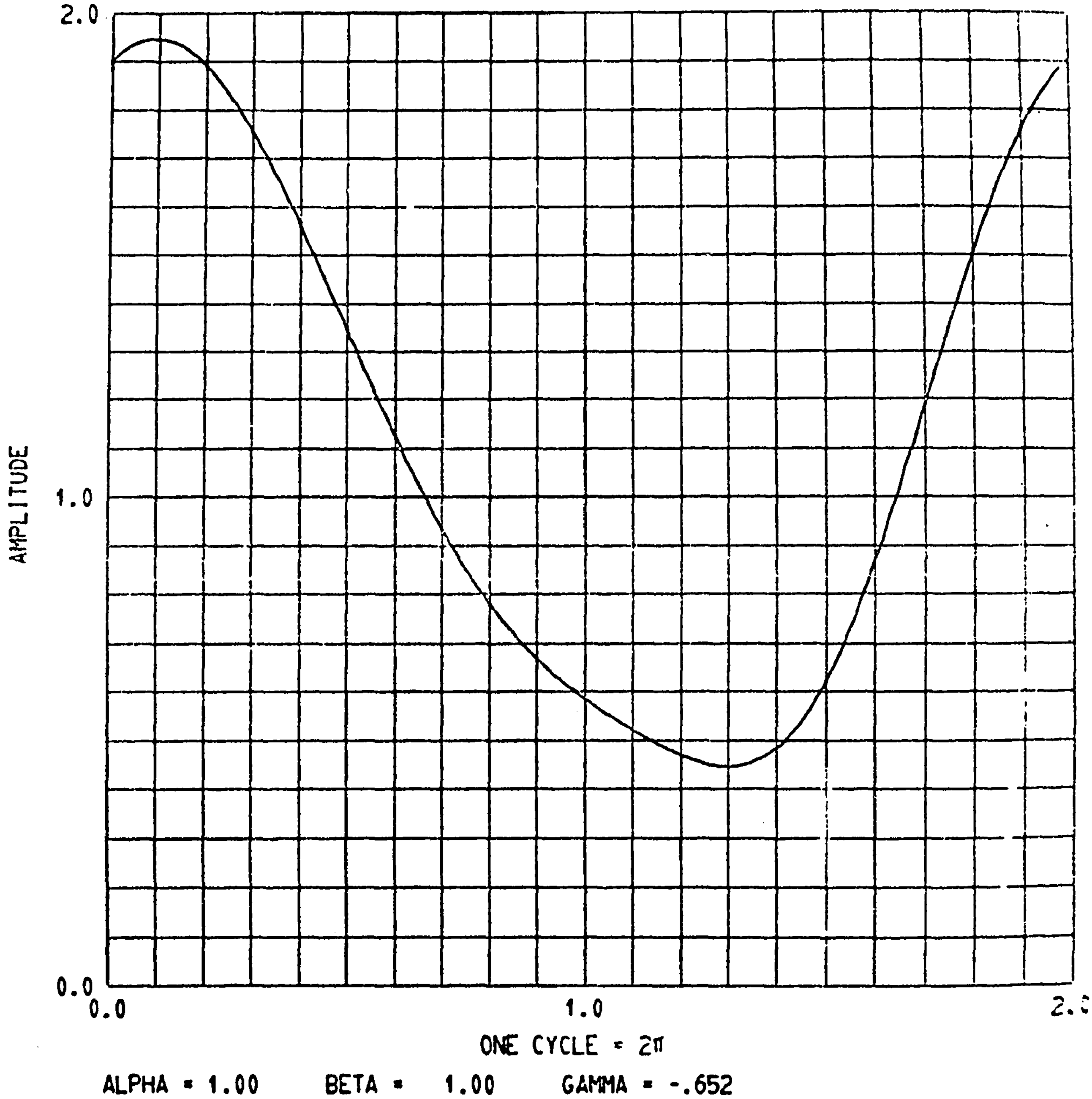

Fig. 20. Output of Eq. (12) when input is a cosine wave.

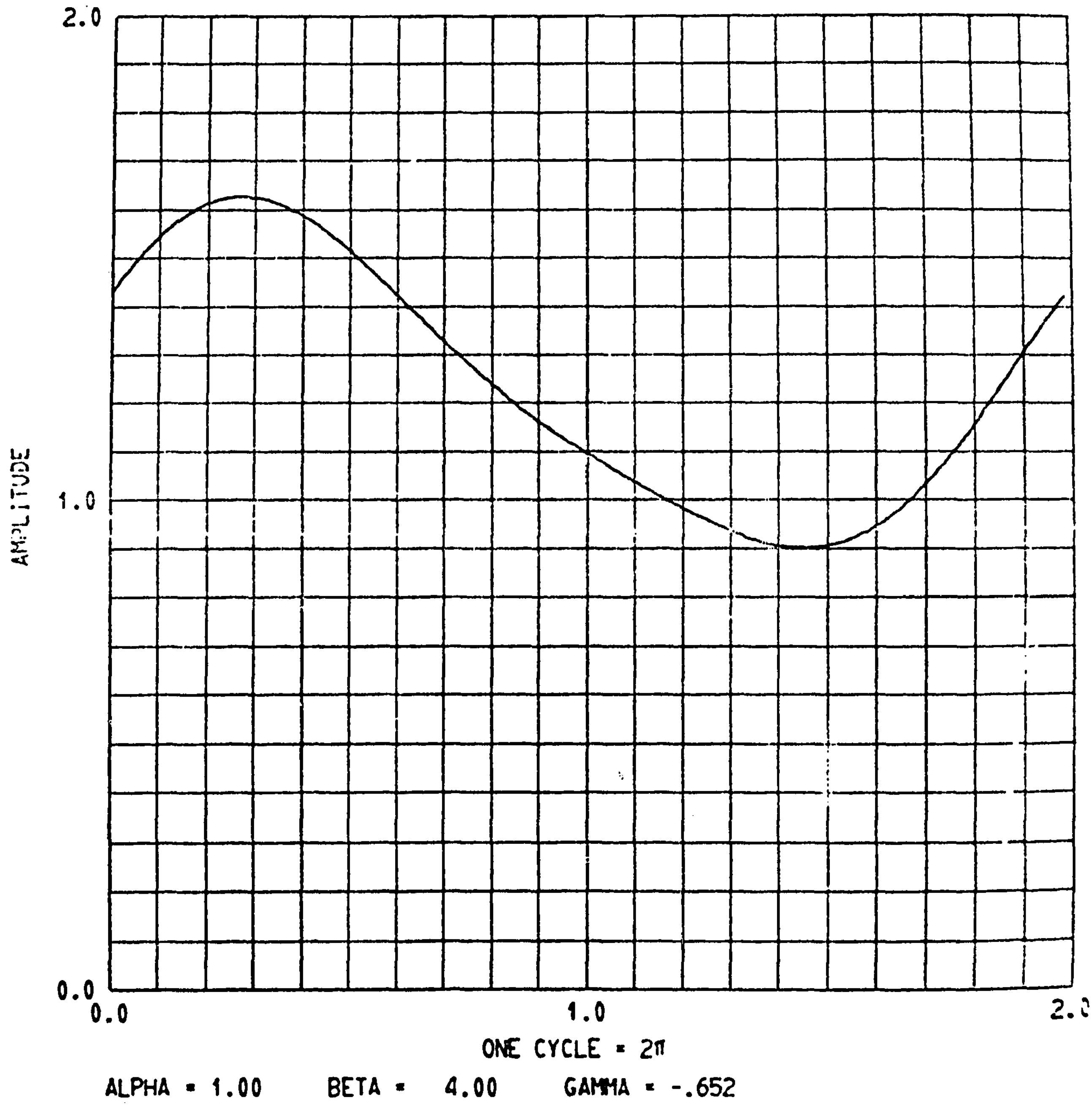

Fig. 21. Output of Eq. (12) when input is a cosine wave.

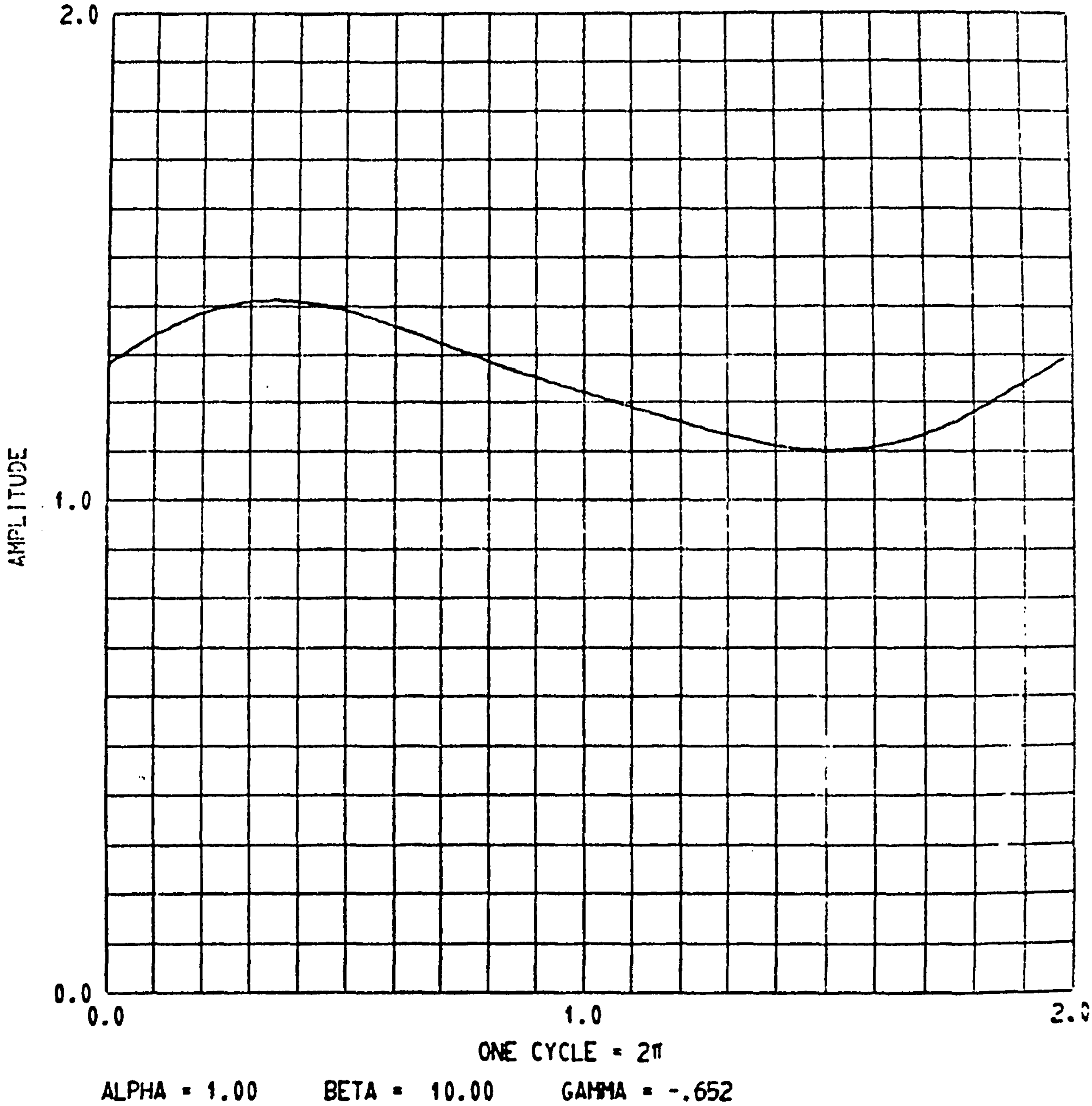

Fig. 22. Output of Eq. (12) when input is a cosine wave.

APPENDIX A

List of Symbols

A(n)	amplitude coefficient
a, b	arbitrary constants
A, B, C	arbitrary constants
E	objective function
f	frequency
H	hot-film anemometer
j	$j^2 = -1$
n	wave number
S	standard propeller anemometer
T	dimensionless time
t	time
U	dimensionless speed
V	anemometer output
V_c	constant wind tunnel speed
V_i	wind speed
W	weighted propeller anemometer
x, y	variables
X, Y	variables
α	model parameter
β	dimensionless frequency
γ	model parameter
Δ	finite increment
λ	distance constant

σ	standard deviation
τ	time constant
φ	phase angle
ω	circular frequency

APPENDIX B

Propeller Anemometer Step Function Response

1. Introduction.

The simplest way to determine the dynamic response of a rotating anemometer is to measure its step response in the wind tunnel and fit a performance model to the data. This requires a performance model that is fairly simple and fits the data reasonably well. It is convenient, and sometimes necessary, to use a linear model because of the immense power of linear systems analysis. The rotating anemometer is not a linear system and it is difficult to fit a linear model to the data objectively. Because of this and because exclusive concern with linear models tends to obscure some markedly nonlinear aspects of anemometer performance, it is desirable to use a nonlinear performance model. Therefore, it seems that both the linear model and a nonlinear model have a place in the deduction of anemometer characteristics.

2. Step function response models.

There is one linear model generally used to describe the dynamic performance of anemometers, and there have been a number of nonlinear models proposed. The following discussion describes the linear model and one versatile nonlinear model from the point of view of step function response. The input, V_i, is the step function with initial conditions as described below.

$$V_i = 0 \text{ for } t < 0$$
$$= V_c \text{ for } t \geq 0$$
$$V(0) = 0$$

The linear model is

$$\lambda \frac{dV}{dt} = V_c(V_c - V) \tag{B1}$$

and its solution for the step function case is

$$V(t) = V_c(1 - e^{-t/\tau}). \tag{B2}$$

where $\tau = \lambda/V_c$.

This model is linear if the input V_c is constant as in the wind tunnel.

The nonlinear model proposed by Kondo, Naito, and Fujinawa (1971), is

$$\lambda \frac{dV}{dt} = (V_c - \gamma V)(V_c - V) \tag{B3}$$

and the solution is

$$\frac{V(t)}{V_c} = \frac{1 - e^{-t/\alpha}}{1 - \gamma e^{-t/\alpha}} \tag{B4}$$

where $\alpha = \lambda/(1 - \gamma)V_c$. Note that if $\gamma = 0$ (B3) is the same as (B1).

3. Test procedure.

The anemometer is mounted in a wind tunnel operating at a constant speed. A brake is applied to stop the anemometer and it is released to start the test. The anemometer responds as though there were a step function increase in the wind speed. The data can be recorded on a strip chart recorder. In abstracting the data it is necessary to carefully determine the level corresponding to the tunnel speed and the start time or moment of release. It is often difficult to determine the start time accurately, especially if the anemometer was not released cleanly. Fig. B1 shows a sample of propeller anemometer step function data. There was noise in the data which, combined with abstraction errors, accounts for the irregularity of the data. Eq. (B2) is the step response for the linear model and shows that the output is 0 until $t = 0$, then increases abruptly and approaches the tunnel speed asymptotically. When $t = \tau$, $V(t)$ is equal to $0.632V_c$. This point is sometimes used as a quick way of determining the time constant τ. It is inappropriate if there is noise present in the data or if the behavior of the system deviates significantly from the performance model. Both conditions obtain in anemometer testing. A good graphical procedure is to plot the data on semi-log paper and fit a straight line to the data. Note that the slope of the line should be equal to $-1/\tau$.

$$\ln\left(1 - \frac{V}{V_c}\right) = -\frac{t}{\tau} \qquad \text{(B5)}$$

Fig. B2 shows the data of Fig. B1 plotted in this way. The curvature of the data is typical of all the step response tests performed on propeller anemometers by the author. The data appear to lie on approximately a straight line for large values of t, in this case for t larger than 1 second. A straight line can be fitted to this portion of the data and a slope determined to give the time constant and the distance constant. There is uncertainty in this procedure because there is no objective way of deciding what data are to be ignored in fitting the straight line.

Fig. B3 shows a plot of (B4), the step function solution of (B3) with the standard linear normalization used above, i.e., the quantity $1 - V/V_c$ is plotted versus time on semi-log paper. When $\gamma = 0$ the solution is the same as for the linear case and yields a straight line whereas $\gamma \neq 0$ yields curved lines. For $\gamma = -0.7$ and $\gamma = -1.0$, the curvature is similar to that observed in Fig. B2.

The value of the parameter γ was chosen arbitrarily to be -1.0 in order to explore the possibility that Eq. (B3) might fit the data better than (B1). If we define $Y = V/V_c$, use the special normalization $(1 - Y)/(1 - \gamma Y)$, and plot on semi-log paper, we obtain from (B4),

$$X = \ln\left(\frac{1 - Y}{1 - \gamma Y}\right) = -t/\alpha. \qquad \text{(B6)}$$

If this model is appropriate and the correct value of γ chosen, the data normalized in this way should scatter about a straight line. In Fig. B4 it can be seen that a straight line can be fitted to all of the data from $t = 0$ through $t = 7$ seconds. The plot does show fluctuation about this straight line; however it was not necessary to exclude any of the data in fitting the line. The nonlinear model is a reasonable fit to the data, and it explains the curvature of the data.

4. Data analysis.

In this section a procedure is shown that can be readily automated, is independent of start time, can be used for the nonlinear model (B3), and includes the linear model (B1) as a special case ($\gamma = 0$). Let $Y = V/V_c$ and use (B6) noting that $\alpha = \lambda/(1 - \gamma)V_c$ becomes $\alpha = \tau$ when $\gamma = 0$. The parameter α can be found by a least squares regression; the approximate numerical equivalent of the graphical procedure described above. Least squares regression of (B6) provides one normal equation

$$\alpha' = - \Sigma Xt/\Sigma X^2$$

where α' is the estimate of α. But if there is a start time uncertainty, t_e, the effect would be to use $t + t_e$ instead of t and that would give

$$\alpha' = - (\Sigma Xt + t_e \Sigma X)(\Sigma X^2)^{-1}$$

so that $- \Sigma Xt/\Sigma X^2$ does not give an unbiased estimate of α. If we use

$$X = \ln\left(\frac{1 - Y}{1 - \gamma Y}\right) = -(t + t_e)/\alpha$$

there would be two normal equations

$$\alpha'' = \frac{\Sigma X \Sigma t - N\Sigma Xt}{N\Sigma X^2 - (\Sigma X)^2} \qquad \text{(B7)}$$

$$t_e = \frac{\Sigma X \Sigma Xt - \Sigma X^2 \Sigma t}{N\Sigma X^2 - (\Sigma X)^2}.$$

It is not necessary to calculate t_e because the equation for α'' will be independent of start time uncertainty, t_e. In addition it is desirable to limit the data used for $\gamma = 0$ to $Y \geq 0.25$, where a straight line fit is more appropriate. This is the approximate cut-off used in the graphical analysis illustrated in Fig. B4. There is a possibility of catastrophic loss of accuracy in this procedure if $Y \geq 1.0$. Due to the presence of noise, Y can exceed 1.0 and so values of $Y \geq 1.0$ must be excluded.

The results are shown in Table B1 for two propeller anemometers, one a standard polystyrene propeller and one which had been weighted.

Table B1. Distance constants for two propeller anemometers.

Anemometer	$\gamma = 0$ (Linear) m	$\gamma = -1$ (Nonlinear) m
Standard	0.98	1.71
Weighted	1.88	3.30

The values obtained for λ in each row of Table B1 are different simply because they come from different models. This illustrates the fact that a parameter such as λ can be defined only in terms of the differential equation model.

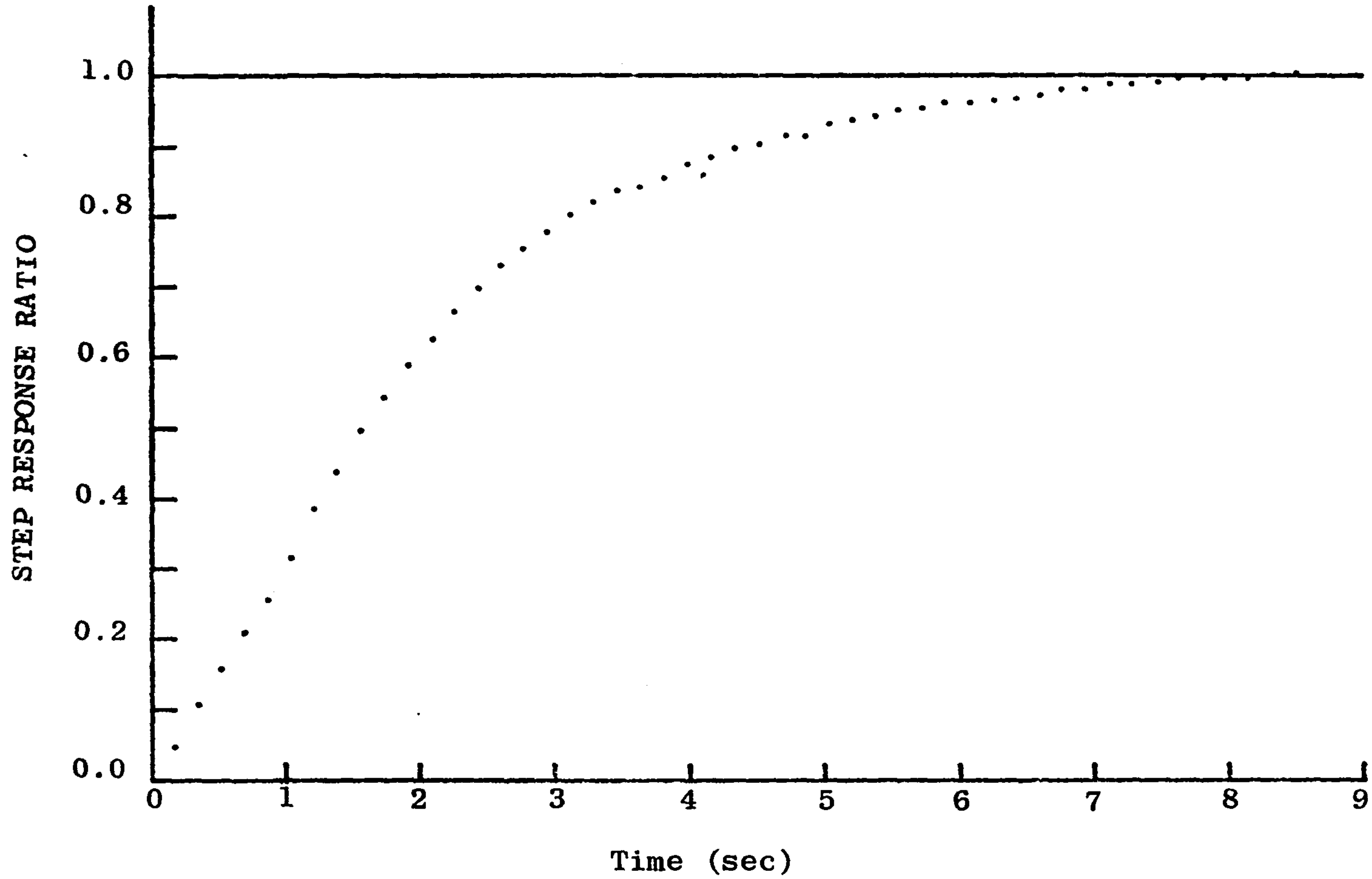

Fig. B1. Sample anemometer step response data. The ratio of anemometer speed to tunnel speed V/V_c is plotted versus time (sec).

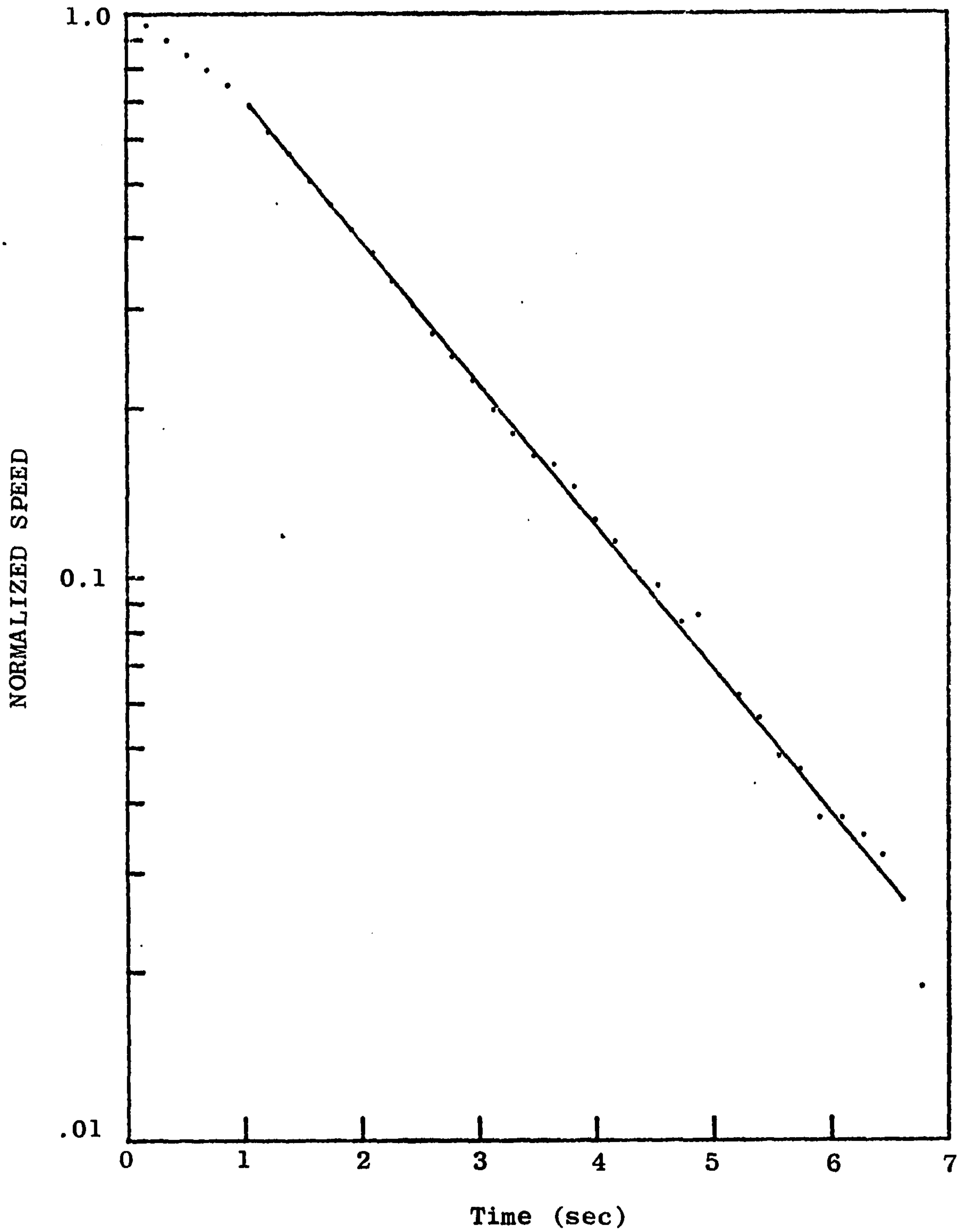

Fig. B2. Anemometer step response data with standard normalization $(1 - V/V_c)$ versus time. The straight line was fitted using data in the range $0.35 \leq V/V_c \leq 0.95$.

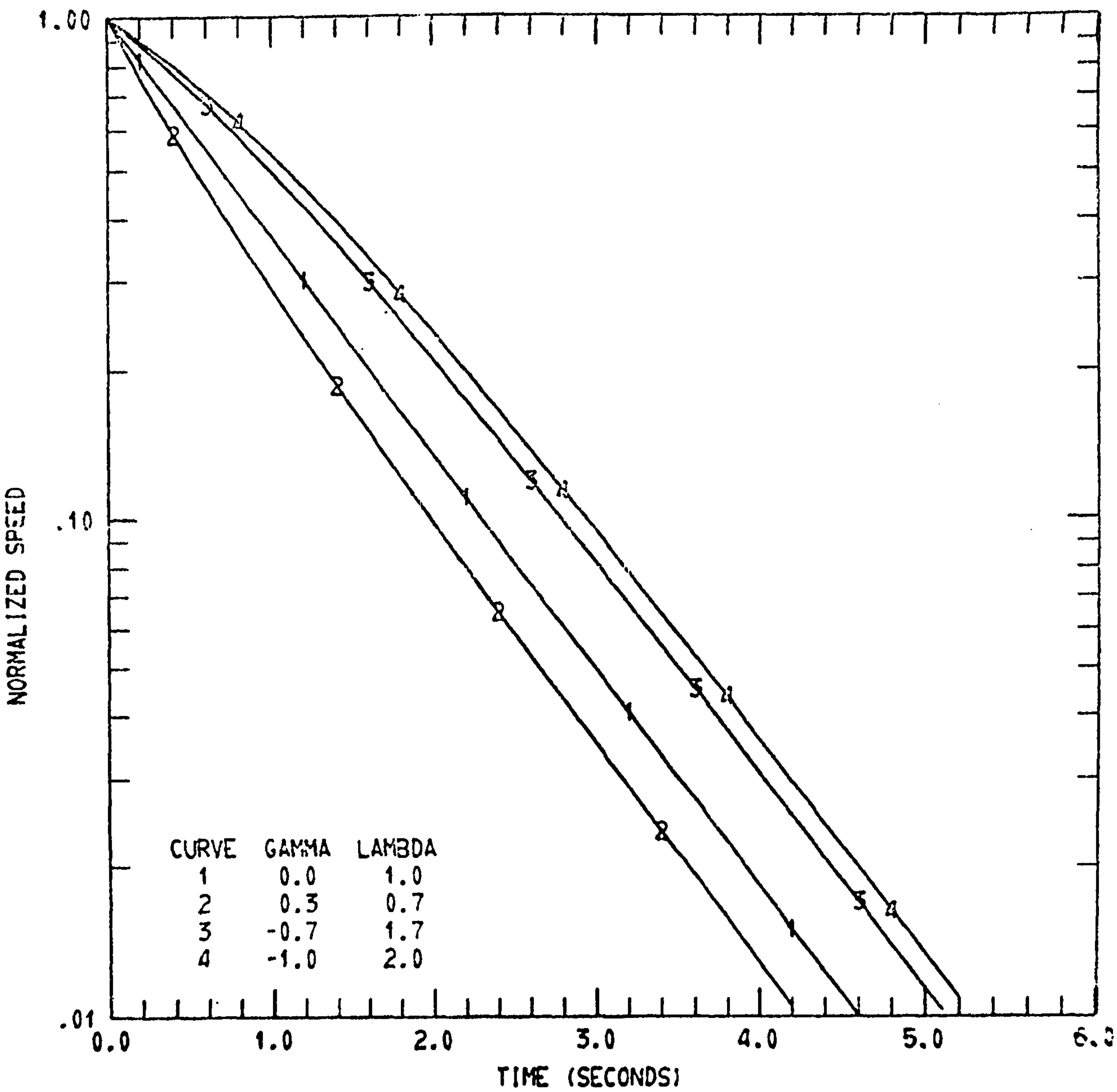

Fig. B3. Plot of (B3) with various values of the parameters γ and λ to show the resulting curvature. The values of λ were chosen to make the lines asymptotically parallel for large values of time.

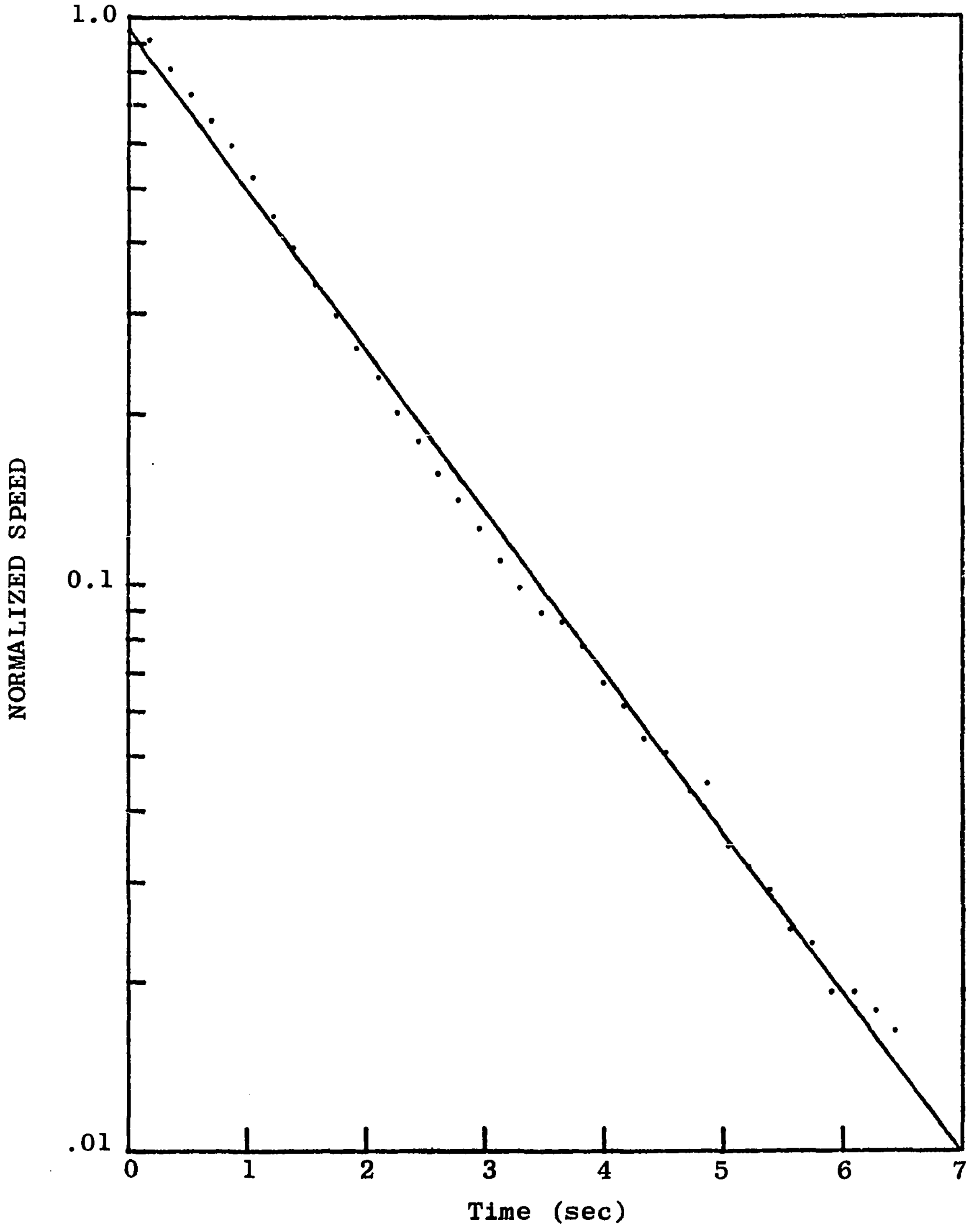

Fig. B4. Anemometer step response data with special normalization $(1 - V/V_c)/(1 + V/V_c)$ which corresponds to $\gamma = -1$. All of the data for which $0 \leq V/V_c < 1$ were used.

APPENDIX C

Simplex Optimization

The simplex optimization scheme described here is a numerical method for multivariable optimization derived from the procedure described by Beveridge and Schechter (1970). The purpose of the scheme is to find the optimum value, in this case the minimum, of some objective function. In this application, the objective function had two parameters and was evaluated from experimental data.

The two-dimensional simplex is an equilateral triangle in the two parameter space (x, y). The objective function E(x, y) is evaluated at each vertex. The optimization procedure consists of rejecting the vertex with the highest value compared to the others. The direction of search is away from the worst vertex along a line through the center of gravity of the other two points. The new point is selected along this line so as to preserve the geometric shape of the figure and then the function is evaluated at the new point. The method proceeds by the process of vertex rejection and regeneration until the figure is in the immediate vicinity of the optimum. Each new simplex requires only one new function evaluation.

The optimization of the two-dimensional function E(x, y) using a sequential simplex method is shown in Fig. C1. The initial simplex is the equilateral triangle with the vertices numbered 1, 2, 3. The optimum is at the point labeled L.

The objective function is evaluated at points 1, 2, and 3. Vertex 1 is rejected since it is the highest (because it is farthest from the low). The new vertex, 4, is chosen and the objective function evaluated there and the procedure is repeated. This simple procedure will fail at a trough line and in the vicinity of the optimum. Consider simplex 11, 12, 13 where the worst vertex is number 11 which will be rejected to form 12, 13, 14. But in this triangle vertex 14 is the worst and application of the above procedure would lead back to triangle 11, 12, 13. To handle this difficulty, a second rule is invoked: no return can be made to a point which has just been left. So instead of rejecting vertex 14 of 12, 13, 14 the second-worst vertex, number 13 is rejected and this leads to the new simplex 12, 14, 15.

Application of this procedure in the vicinity of the optimum will cause the simplex to rotate about the vertex with the best value. The rotated simplex pattern is shown in Fig. C1 where the initial triangle of the pattern is 10, 11, 12 and the final one is 10, 12, 16. The search procedure is stopped when rotation occurs and then the best approximation to the optimum is the pivot vertex.

The approximation can be improved by reducing the size of the simplex and starting over from the last approximation.

Another way is to fit a quadratic surface to the seven points of the rotated simplex. This does not require any additional function evaluations. A quadratic surface

$$\Delta E = a_o X + a_1 Y + a_2 XY + a_3 X^2 + a_4 Y^2 \tag{C1}$$

can be fitted to the data where the vertex of rotation is at x_o, y_o with value E_o. Then for any of the rotated simplex vertices, $X = x - x_o$, $Y = y - y_o$ and $\Delta E = E - E_o$. Since there are five unknowns in (C1) and seven sets of data, the coefficients can be evaluated by least squares. Then the location of the optimum can be found from

$$\left.\begin{aligned} \frac{\partial(\Delta E)}{\partial X} &= a_o + a_2 Y + 2a_3 X = 0 \\ \frac{\partial(\Delta E)}{\partial Y} &= a_1 + a_2 X + 2a_4 Y = 0 \end{aligned}\right\} \tag{C2}$$

which yields

$$\left.\begin{aligned} x_1 &= x_o + (2a_o a_4 - a_1 a_2)(a_2{}^2 - 4a_3 a_4)^{-1} \\ y_1 &= y_o + (2a_1 a_3 - a_o a_2)(a_2{}^2 - 4a_3 a_4)^{-1} \end{aligned}\right. \tag{C3}$$

where x_1, y_1 is the improved estimate of the location of the optimum.

The optimization scheme can fail in several interesting ways. The simplex could rotate at a point far from the optimum. A relatively large triangle can rotate in the vicinity of a narrow trough even when the optimum is not in the vicinity. This can also lead to failure of the quadratic approximation which tends to fail if the data are taken far from the optimum or if there are small irregularities in the field being evaluated. Due to combinations of these effects it is possible for the simplex figure to rotate and for the subsequent quadratic approximation to yield a point within the boundary of the rotated simplex while the optimum is still far away.

With the addition of some control features to the above logic it is possible to avoid most of the traps and have an optimizing scheme which is almost completely automatic. But there will probably always be situations where successful optimization will require human guidance. The additional controls required are a definition of an allowable range of parameter values, a limit on the number of iterations of sequential simplexes, and halving the triangle size until the quadratic approximation falls within the rotated simplex. The last condition should be reimposed until the simplex size is reduced below some specified maximum size.

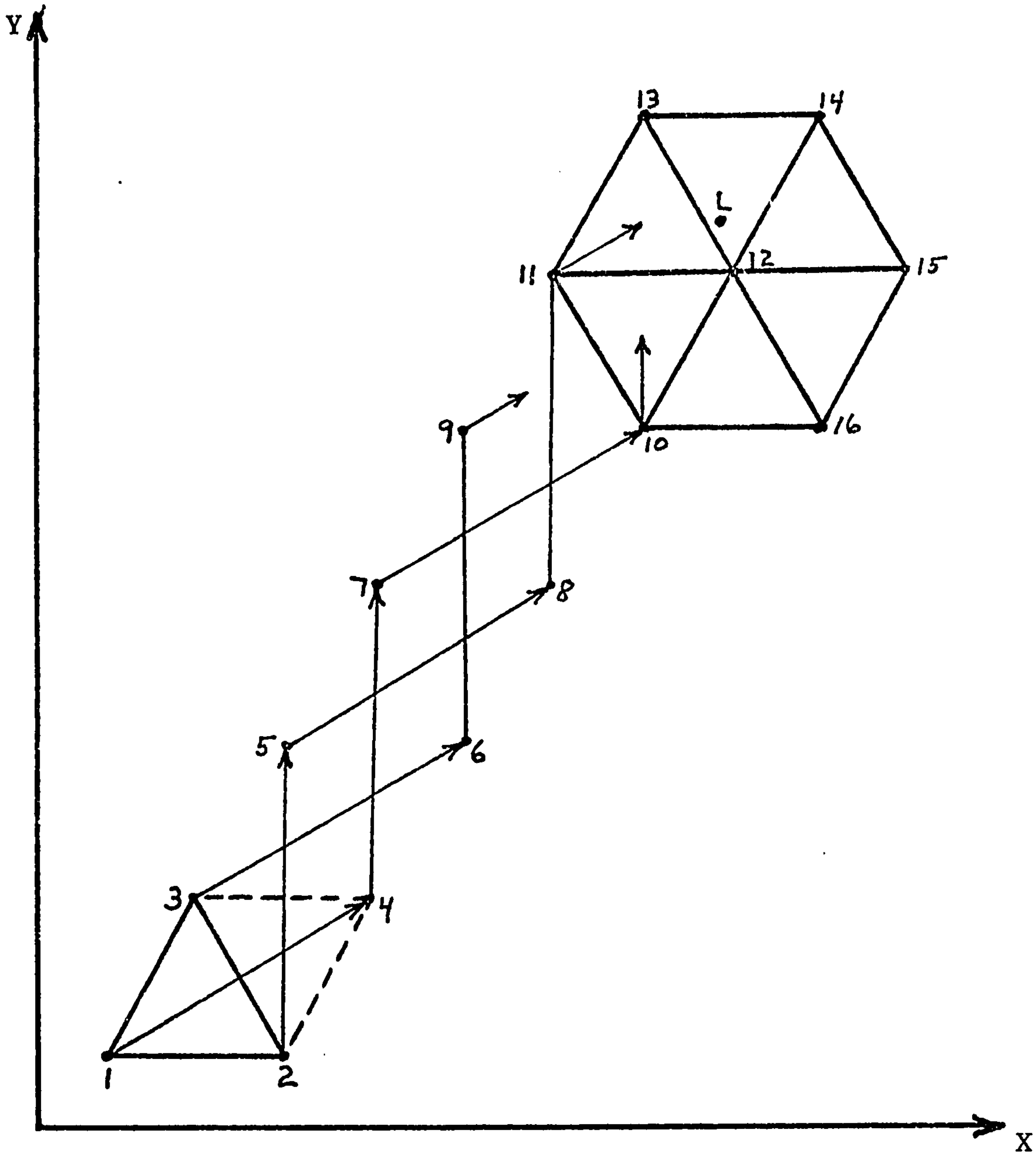

Fig. C1. Illustration of sequential simplex optimization. The optimum is at point L.

REFERENCES

Acheson, Donald T., 1970: Response of cup and propellor rotors and wind direction vanes to turbulent wind fields. Meteorological Monographs, 11, No. 33, 252-261.

Beveridge, Gordon S. G. and Robert S. Schechter, 1970: Optimization: Theory and Practice. New York, McGraw-Hill Book Co., 773 pp.

Hyson, P., 1972: Cup anemometer response to fluctuating wind speeds. Jour. Appl. Meteor. 11, 843, 848.

Izumi, Yutaka and Morton L. Barad, 1970: Wind speeds as measured by cup and sonic anemometers and influenced by tower structures. Jour. Appl. Meteor., 9, 851-856.

Kondo, Junsei, Gen-ichi Naito and Yukio Fujinawa, 1971: Response of cup anemometers in turbulence. J. Met. Soc. Japan, 49, 63-74.

MacCready, Paul B., Jr., 1970: Theoretical considerations in instrument design. Meteorological Monographs, 11, No. 33, 202-210.

Pike, Julian M., 1970: A calibration facility for meteorological instruments. Instr. Soc. Amer. Conference ISA-70, paper No. 718-70.

Ramachandran, S., 1969: A theoretical study of cup and vane anemometers. Quart. J. Roy. Met. Soc., 95, 163-180.

Schubaer, G. B., and G. H. Adams, 1954: Lag of anemometers, Report #3245, N.B.S., U.S. Department of Commerce, Washington, D. C.

Thompson, Robert J., 1970. Improving round-off error in Runge-Kutta computation with Gill's method. Comm. ACM, Vol. 13, No. 12, pp. 739-740.